Biomedicine & Pharmacotherapy 191 (2025) 118439

Contents lists available at ScienceDirect

Biomedicine & Pharmacotherapy

journal homepage: www.elsevier.com/locate/biopha

Soluble guanylate cyclase stimulation improves cardiac function and mitochondrial activity in a rat model of early-stage heart failure with preserved ejection fraction

Xocas Vázquez-Abuín [a,b,1], Sandra Moraña-Fernández [a,c,1], Alana Aragón-Herrera [a,b,*,2], Peter Sandner [d], Karen Thomitzek [e], Javier García-Seara [a,b,f,g,h], Susana B. Bravo [i], Manuel Otero-Santiago [a,j], Pablo de la Fuente-López [a,h], Carlos Tilves-Bellas [h], Alexandre Rodrigues [k], Alexandre Gonçalves [k], Juliana Pereira Morais [l], Inês N. Alves [k], Cláudia Sousa-Mendes [k], Inês Falcão-Pires [k], Estefanía Tarazón [b,m], Esther Roselló-Lletí [b,m], Manuel Portolés [b,m], Oreste Gualillo [n], José Ramón González-Juanatey [a,b,g,h], Sandra Feijóo-Bandín [a,b,1], Francisca Lago [a,b,1]

[a] *Cellular and Molecular Cardiology Research Unit, IDIS, Complexo Hospitalario Universitario de Santiago de Compostela, Área Sanitaria Santiago de Compostela e Barbanza (SERGAS), Santiago de Compostela, Spain*
[b] *Centro de Investigación Biomédica en Red de Enfermedades Cardiovasculares (CIBERCV), Instituto de Salud Carlos III, Madrid, Spain*
[c] *Center for Research in Molecular Medicine and Chronic Diseases (CIMUS), Universidade de Santiago de Compostela, IDIS, Complexo Hospitalario Universitario de Santiago de Compostela, Santiago de Compostela, Spain*
[d] *Bayer AG, Pharmaceuticals, Cardiovascular & Renal Research, Wuppertal, Germany*
[e] *Bayer AG, Pharmaceuticals, Medical Affairs Cardiovascular and Haematology, Berlin, Germany*
[f] *Arrhytmia Unit, Cardiology Department, IDIS, Complexo Hospitalario Universitario de Santiago de Compostela, Área Sanitaria Santiago de Compostela e Barbanza (SERGAS), Santiago de Compostela, Spain*
[g] *Department of Psychiatry, Radiology, Public Health, Nursing and Medicine, IDIS, Universidade de Santiago de Compostela, Santiago de Compostela, Spain*

Abbreviations: AA,, Amino Acids; ADT1,, ADP/ATP Translocase 1; AATM,, Aspartate Aminotransferase Mitochondrial; Ant1,, Adenine Nucleotide Translocator 1 ADP/ATP Translocase 1 gene; Asc,, Ascorbate; ATP,, Adenosine Triphosphate; AT5F1,, ATP Synthase F0 Complex Subunit B1, Mitochondrial; ATPG,, ATP Synthase Subunit Gamma, Mitochondrial; BA,, Bile Acids; BIOPS,, Relaxing and Biopsy Preservation Solution; BNP,, B-type Natriuretic Peptide; CCCP,, Carbonyl Cyanide m-Chlorophenyl Hydrazone; CGMP,, Cyclic Guanosine Monophosphate; CO,, Cardiac Output; CYB5B,, Cytochrome B5 Type B; E,, Early Diastolic Transmitral Flow Velocity; EF,, Ejection Fraction; EF-TU_{mt},, Elongation Factor Thermal Unstable Tu, Mitochondrial; E',, Peak Early Diastolic Velocity; ES1,, ES1 Protein Homolog, Mitochondrial; FDR,, False Discovery Rate; FMUP,, Faculty of Medicine of the University of Porto; FS,, Fractional Shortening; Glp,, Glycerophosphate; GC,, Guanylate Cyclase; HR,, Heart Rate; H&E,, Hematoxylin and Eosin; HF,, Heart Failure; HFrEF,, Heart Failure with Reduced Ejection Fraction; HFpEF,, Heart Failure with Preserved Ejection Fraction; IDHG1,, Isocitrate Dehydrogenase [NAD] Subunit Gamma 1, Mitochondrial; IVRT,, Isovolumetric Relaxation Time; L-NAME,, Nω-Nitro-L-arginine Methyl Ester; LVIDd,, Left Ventricular Internal Diameter in Diastole; LVIDs,, Left Ventricular Internal Diameter in Systole; LVEDV,, Left Ventricular End-Diastolic Volume; LVESV,, Left Ventricular End-Systolic Volume; LV,, Left Ventricle; M,, Malate; MAP4,, Microtubule-Associated Protein 4; MCU,, Mitochondrial Calcium Uniporter; MetS,, Metabolic Syndrome; MICU1,, Mitochondrial Calcium Uptake 1; MICU2,, Mitochondrial Calcium Uptake 2; MDHM,, Malate Dehydrogenase Mitochondrial; MS,, Mass Spectrometry; MS1,, Precursor Ion Scan MS1 Spectrum; MS2,, Fragment Ion Scan MS2 Spectrum; NDUA9,, NADH Dehydrogenase [Ubiquinone] 1 Alpha Subcomplex Subunit 9, Mitochondrial; NDUAA,, NADH Dehydrogenase [Ubiquinone] 1 Alpha Subcomplex Subunit 10, Mitochondrial; NDUAB,, NADH Dehydrogenase [Ubiquinone] 1 Alpha Subcomplex Subunit 11; NDUS1,, NADH-Ubiquinone Oxidoreductase 75 kDa Subunit, Mitochondrial; NDUV2,, NADH Dehydrogenase [Ubiquinone] Flavoprotein 2, Mitochondrial; NO,, Nitric Oxide; Oct,, Octanoylcarnitine; OD,, Once Daily; OXPHOS,, Oxidative Phosphorylation; P,, Pyruvate; Pfi,, Permeabilized Fibers; PRDX3,, Thioredoxin-Dependent Peroxide Reductase, Mitochondrial; PRDX5,, Peroxiredoxin-5, Mitochondrial; PRDX6,, Peroxiredoxin-6; PPP,, Pentose Phosphate Pathway; RT,, Room Temperature; SGLT2,, Sodium-Glucose Cotransporter-2; SLC25A4,, Solute Carrier Family 25 Member 4 ADP/ATP Translocase 1 gene; SDHA,, Succinate Dehydrogenase [Ubiquinone] Flavoprotein Subunit, Mitochondrial; SODM,, Superoxide Dismutase [Mn], Mitochondrial; SGC,, Soluble Guanylate Cyclase; SWATH,, Sequential Window Acquisition of all Theoretical Mass Spectra; SUIT,, Substrate-Uncoupler-Inhibitor Titration; TAPSE,, Tricuspid Annular Plane Systolic Excursion; TBB4B,, Tubulin Beta-4B Chain; TL,, Tibia Length; TMOD1,, Tropomodulin 1; TMPD,, N,N,N,N-Tetramethyl-p-Phenylenediamine; TOM70,, Translocase of Outer Mitochondrial Membrane 70; TPM1,, Tropomyosin Alpha-1 Chain; UHPLC-MS,, Ultra-High Performance Liquid Chromatography Coupled to Mass Spectrometry; VDAC3,, Voltage-Dependent Anion-Selective Channel Protein 3; ZSF1,, Zucker Fatty and Spontaneously Hypertensive; 6PGL,, 6-Phosphogluconolactonase; 6PGDH,, 6-Phosphogluconate Dehydrogenase.

* Correspondence to: Laboratorio 7, Instituto de Investigaciones Sanitarias de Santiago de Compostela (IDIS), Hospital Clínico Universitario de Santiago de Compostela, Travesía Choupana s/n, Santiago de Compostela 15706, Spain.
E-mail address: alana.aragon.herrera@sergas.es (A. Aragón-Herrera).

https://doi.org/10.1016/j.biopha.2025.118439
Received 12 May 2025; Received in revised form 28 July 2025; Accepted 6 August 2025
Available online 12 August 2025

[h] Cardiology Department, IDIS, Complexo Hospitalario Universitario de Santiago de Compostela, Área Sanitaria Santiago de Compostela e Barbanza (SERGAS), Santiago de Compostela, Spain
[i] Proteomic Unit, Health Research Institute of Santiago de Compostela (IDIS), Santiago de Compostela, Spain
[j] Clinical Biochemistry Laboratory, Área Sanitaria Santiago de Compostela e Barbanza (SERGAS), Santiago de Compostela, Spain
[k] Cardiovascular R&D Centre - UnIC@RISE, Department of Surgery and Physiology, Faculty of Medicine, University of Porto, Porto, Portugal
[l] CINTESIS@RISE, NOVA Medical School|Faculdade de Ciências Médicas, NMS|FCM, Universidade Nova de Lisboa, UnIC@RISE - Cardiovascular Research Centre, Faculdade de Medicina, Universidade do Porto, Porto, Portugal
[m] Cardiocirculatory Unit, Health Research Institute of La Fe University Hospital, Valencia, Spain
[n] Laboratory of Neuroendocrine Interactions in Rheumatology and Inflammatory Diseases, IDIS, Complexo Hospitalario Universitario de Santiago de Compostela, Santiago de Compostela, Spain

ARTICLE INFO

Keywords:
Soluble guanylate cyclase stimulator
Heart failure with preserved ejection fraction
Proteome
Diastolic dysfunction
Mitochondria
ZSF1

ABSTRACT

Targeting cardiac mitochondrial dysfunction and cardiac metabolic reprogramming is critical for improving chronic heart failure (HF) treatment. While the soluble guanylate cyclase stimulator vericiguat has shown promise in treating HF with reduced ejection fraction (HFrEF), its effects on HF with preserved ejection fraction (HFpEF), particularly on myocardial bioenergetics, remain undefined. This study aimed to clarify the effects of vericiguat on cardiac function and metabolism in a preclinical model of early-stage HF. Obese ZSF1 (Zucker fatty and spontaneously hypertensive) rats were randomized to receive standard care (n = 10) or vericiguat (3 mg/kg/d p.o.) (n = 10) treatment for 4 weeks. ZSF1 lean rats (n = 10) served as controls. Vericiguat improved diastolic function, reduced cardiac hypertrophy and fibrosis and enhanced cardiac mitochondrial basal respiration, upregulating the levels of several mitochondrial electron transport chain proteins from complexes I, II, III and V, along with the ADP/ATP translocase 1 mRNA levels, and partially reversing mitochondrial cristae diffuse dissolution observed in obese control rat hearts. Vericiguat treatment increased cardiac levels of phosphoproteins involved in the pentose phosphate pathway (PPP) (6-phosphogluconolactonase and 6-phosphogluconate dehydrogenase) and in the Krebs cycle (malate dehydrogenase and aspartate aminotransferase), while normalizing the mRNA levels of the master regulator of calcium uptake by the mitochondria (MICU1). Furthermore, vericiguat restored the cardiac levels of key metabolites of the PPP such as 6-phosphogluconate, D-ribose 5-phosphate, and arginine, that were diminished in the obese control group. In conclusion, vericiguat elicits beneficial functional and metabolic responses at cardiac level in an animal model of early-stage HFpEF.

1. Introduction

The nitric oxide (NO)-soluble guanylate cyclase (sGC)-cyclic guanosine monophosphate (cGMP) pathway plays a crucial role in the regulation of cardiac functionality and protection of the heart; in fact, dysfunctional NO-sGC-cGMP signalling could result in heart failure (HF) [1–4]. Vericiguat is a stimulator of sGC with a dual mode of action: it can trigger cGMP production by binding and stimulation of sGC in synergy, but also independent of endogenous NO [5,6]. In non-clinical models, vericiguat effectively reduced mortality and vascular stiffness, suggesting a beneficial effect in HF treatment [7–9]. In fact, vericiguat reduced the risk of CV death and HF hospitalization in HF patients with reduced ejection fraction (HFrEF), but had less pronounced effect in HF patients with preserved ejection fraction (HFpEF) [10–14]. Therefore, to fully understand the mode of action of sGC stimulators in HF and the therapeutic spectrum of vericiguat, additional non-clinical and subsequent clinical studies are required. Investigating the potential effects of sGC stimulators on the various pathophysiological mechanisms leading to HF may, in turn, support more personalised HF management. This is particularly important in HFpEF, where oxidative stress-dependent alterations of the NO–sGC–cGMP pathway (a crucial regulator of cardiac contraction and relaxation; [15]) are involved in the pathophysiology of myocardial dysfunction [16–18]. In HFpEF, the sGC stimulators vericiguat and praliciguat failed in phase 2 clinical trials, a finding that remains insufficiently understood, given that oxidative stress-induced endothelial dysfunction in HFpEF could, in principle, be ameliorated by sGC stimulators [13,19]. In accordance with this, a sex-specific beneficial electrophysiological response to vericiguat in cardiomyocytes from an experimental model of obese diabetic mice with HFpEF has been demonstrated [20]. While HFpEF may arise from various aetiologies, its progression is primarily driven by metabolic dysfunctions such as obesity and diabetes, which induce deleterious alterations in mitochondrial energy metabolism [21,22]. The potential impact of treatment with the sGC stimulator vericiguat on myocardial bioenergetics in chronic HF and HFpEF has not yet been defined, and elucidating the mechanistic basis for vericiguat's effects in these conditions warrants further research. The aim of this work is to clarify the effects of the treatment with vericiguat on cardiac function and metabolism using a preclinical model of HFpEF, the Zucker fatty and spontaneously hypertensive (ZSF1) rats. Adult ZSF1 rats at an early-stage of HFpEF (14 weeks of age) were treated with the sGC stimulator vericiguat for 4 weeks. Cardiac function was assessed by echocardiography, while cardiac tissue was characterised using histomorphological and electron microscopy techniques, alongside metabolomic and proteomic analyses and high-resolution respirometry. Our data suggests that vericiguat treatment may elicit beneficial functional and metabolic responses in the heart of ZSF1 rats at an early-stage of HFpEF. Vericiguat improved diastolic dysfunction, reduced hypertrophy and fibrosis, ameliorated mitochondrial function, increased levels of pivotal mitochondrial proteins involved in antioxidant processes, and stimulated cardioprotective metabolic processes.

2. Methods

All reagents employed are from Sigma-Aldrich (USA) otherwise indicated.

2.1. Ethical approval

All experimental procedures employing animals are described according to the Guide for the Care and Use of the Laboratory Animals published by the National Institutes of Health [23]. The study protocol was approved by the ethics committee of the Faculty of Medicine of the University of Porto (FMUP), the FMUP Animal Welfare and Ethics Review Body (Orgão de Bem-Estar e Ética Animal), and by the Portuguese Direçao-General de Alimentaçao e Veterinária (8161/23S). The FMUP is

[1] These two authors contributed equally
[2] ORCID: 0000–0003-3089–0684

approved by de Portuguese government to perform animal experiments. The number of animals used in the experimental procedures was the minimal necessary to develop our objectives and to ensure a pertinent statistical power.

2.2. Animals

Adult male obese (440–520 g) and lean (300–380 g) Zucker fatty and spontaneously hypertensive (ZSF1) rats were purchased from Charles River Laboratories International, Inc. (USA) at 13 weeks of age. This animal model is adequate for our experiment since it represents a well-established model of metabolic syndrome (MetS) that, at 20 weeks, presents the characteristic phenotype of HFpEF along with many comorbidities: exercise intolerance, chronic kidney disease, damaged endothelial function, etc [24,25]. Rats were housed in pairs in cages under controlled conditions of room temperature (RT) (22 ºC), relative humidity (55 ± 10 %) and illumination (inverted 12-hour light/dark cycles, lights off at 08:00 and lights on at 20:00) in the Animal House of the Faculdade de Medicina do Porto (FMUP, PRT). They were maintained with *ad libitum* access to the special Formulab 5008 diet for rodents (4.15 kCal/g; 23 % protein, 6, 5 % fat, 58.5 % carbohydrates, 4 % fibre and 8 % ash) (Research Diets Inc., USA) and mineral drinking water. Food and water intake, and body weight were measured weekly. At the end of the treatment, animals were euthanized under sevoflurane-anaesthesia (8 %) (AbbVie, USA) via inhalation by exsanguination, and organs were collected, weighed, quickly frozen in liquid nitrogen, and stored at −80 °C until subsequent analysis. Organ weights were normalised to the tibia length due to body weight differences between the groups [26]. For histological analysis, samples were stored in buffered 10 % formaldehyde. For mitochondrial respiration studies, a tiny sample of the left ventricle (LV) was stored in biopsies until use. Blood samples were collected in spray-coated K_2EDTA and SST Advance tubes (BD Vacutainer®, USA), and centrifuged at 5000 rpm for 15 min at 4 °C. The plasma and serum samples were collected in aliquots and frozen at −80ºC until subsequent analysis.

2.3. Vericiguat in vivo treatment

Rats were treated at 14 weeks of age for 4 weeks with the sGC stimulator Vericiguat (Bayer AG, DEU) given at a dose of 3 mg/kg administered once daily (OD), orally (p.o.), in an aqueous suspension with a syringe [27]. Body weight was measured once a week to adjust the treatment dose according to weight changes. Rats were randomly divided into 3 groups: obese control group (vehicle, mineral drinking water) (n = 10), lean control group (vehicle, mineral drinking water) (n = 10), and obese vericiguat group (n = 10), with *n* defined as independent animal individuals.

2.4. Metabolic characterization

Urine and stool production was noninvasively assessed at 17 weeks of age by housing the animals for 24 h in metabolic cages (Techniplast, ITA). Animals were previously adapted to the new environmental conditions (individualization of animals, cage size and food and drink systems). Urine samples were collected and centrifuged at 5000 rpm for 15 min at 4 °C. The supernatant was collected in aliquots and was frozen at −80ºC until subsequent analysis.

2.5. Echocardiography

At 17 weeks of age (3 weeks of treatment), the echocardiographic evaluation was performed under sevoflurane anaesthesia (4 %). Cardiac structure and function were determined by transthoracic echocardiography using the Acuson Sequoia C512 (Siemens Healthineers, DEU), equipped with a linear 15 MHz probe Sequoia 15L8W (Siemens Healthcare Diagnostics, DEU), positioned over the thorax [28]. M-mode was used to determine LV internal diameter in diastole (LVIDd) and systole (LVIDs) in parasternal short-axis view. From these values, fractional shortening (FS) can be calculated, applying the following formula:

FS (%) = (LVIDd-LVIDs)/LVIDd x 100

M-mode was also used to determine the tricuspid annular plane systolic excursion (TAPSE), a reliable parameter to assess global right ventricle function, in the apical four-chamber view. B-mode was used to determine left ventricular end-diastolic (LVEDV) and systolic (LVESV) volume parasternal long-axis view. Based on these calculations, parameters such as stroke volume (SV) (volume of blood ejected from the LV during systole), and cardiac output (CO) (volume of blood ejected from the LV per minute), can be determined applying the following formulas:

EF (%) = (LVEDV-LVESV)/LVEDV x 100,

SV (mL) = (LVEDV-LVESV),

CO (mL/min) = SV x HR.

Diastolic parameters like isovolumic relaxation time (IVRT), late diastolic transmitral flow velocity (A), and early diastolic transmitral flow velocity (E) were obtained with pulsed-wave Doppler. Heart rate (HR) was obtained with pulsed-wave Doppler in the apical five-chamber view. Recordings were averaged from 3 consecutive heartbeats. Echocardiograph data analysis was performed using the software Syngo US Workplace Software (Siemens Healthineers, DEU).

2.6. Quantitative histomorphometry

After fixation with buffered 10 % (v/v) formaldehyde, histological samples were embedded in paraffin and cut into sections of 3 μm of thickness. Histomorphological analysis of heart samples was performed with picro-sirius red and hematoxylin and eosin (H&E). H&E staining was used to quantify cardiomyocytes area as an indicator of hypertrophy. Sections were digitally photographed (Olympus XC30, Olympus, JPN). Digital images (magnification of x40) were analysed using image analysis software (Cell B Software Version 3.4, Olympus, JPN). Sixty randomly selected cardiomyocytes were analysed per sample. Picro-sirius red staining was used to quantify fibrosis. Sections were digitally photographed (Zeiss Axio Scope A1, Zeiss, DEU). Digital images (magnification of x20) were analysed using image analysis software (Image-Pro Plus version 6.0, Media Cybernetics Inc., USA). Six randomly selected fields were analysed per sample [29,30].

2.7. Transmission electron microscopy

After LV tissue collection, the samples were immediately fixed in 2.5 % glutaraldehyde in cacodylate buffer and post-fixed in osmium tetroxide. The tissue samples were then dehydrated in graded ethanol (95 –100 %), and subsequently embedded in a mixture of polypropylene oxide with Epon resin at RT. Then the samples were placed in Epon resin blocks and placed at 60°C for 2–3 days. Ultrathin sections (80 nm) were performed in an ultramicrotome Leica Ultracut UCT (Leica Microsystems GmbH, DEU), and were contrasted with uranyl acetate and lead citrate in a Leica EM AC20 (Leica Microsystems GmbH, DEU) automatic contrasting instrument. The grids were examined under a transmission electron microscope JEOL JEM 1011 (JEOL Ltd., JPN) at 80 KV with a ×5000 and ×30000 magnification, and images were photographed with a MegaView G3 camera (Media System Lab S.r.l., ITA) in the Microscopy Service of the University of Santiago de Compostela (USC) in Spain. Images were analysed with ImageJ software (Version 1.54 g) (USA). For each sample, 5 randomly chosen fields with a ×30000 magnification were employed. A total of 125–148 mitochondria were analysed from 4 LV samples of each group. Mitochondria cristae destruction classification was scored as 0 = absent, 1 = mild, 2 = moderate/severe.

2.8. Mitochondrial oxygen consumption rate evaluation

The evaluation of the oxygen consumption rate of mitochondria from LV permeabilized fibres (pfi), during different states of coupling control, was performed using a High Resolution FluoRespirometer O2k (Oroboros Instruments GmbH, AUT), with the substrate-uncoupler-inhibitor titration (SUIT) protocol for pfi. SUIT-001 O2 pfi protocol allowed to assess mitochondria specific flux (the mitochondrial respiration normalised by the sample mass) during basal respiration; non-phosphorylating state (LEAK) in the absence of adenosine diphosphate (ADP); OXPHOS state activated in the presence of saturating concentrations of ADP [1–5 mM]; and maximal electron transfer capacity after titration with the uncoupler carbonyl cyanide m-chlorophenyl hydrazone (CCCP) as previously described [31,32]. Briefly, LV tissue was submerged in an ice-cold relaxing and biopsy preservation solution (BIOPS) [10 mM Ca-EGTA buffer (2.77 mM CaK2EGTA + 7.23 mM K2EGTA; 0.1 μM free calcium), 50 mM K+ -MES, 20 mM taurine, 0.5 mM dithiothreitol, 6.56 mM MgCl2, 5.77 mM ATP, 15 mM phosphocreatine and 20 mM imidazole; pH = 7.1 adjusted with 5 N KOH at 0 °C] for mechanical separation of cardiac fibres. Afterwards, LV fibres were immersed for 30 min in 2 mL of ice-cold saponin and BIOPS solution (5 mg saponin /1 mL BIOPS) for its permeabilization and, subsequently, acclimatized to the procedure medium MIR06 [MIR05 (MiR05-Kit, Oroboros Instruments GmbH, AUT) with 280 U/mL catalase] for 15 min. Following permeabilization, 1–2 mg of LV pfi were added into each chamber of the FluoRespirometer with 2.0 mL of MIR06 medium. The addition of different substrates and inhibitors enables the assessment of each segment of the electron transport chain: complex I (pyruvate (P) [5 mM] + malate (M) [2 mM], glutamate [10.0 mM] and rotenone [0.5 μM]); complex II (succinate [50.0 mM]); complex III (antimycin A [2.5 μM]) and complex IV (N,N,N,N-Tetramethyl-p--phenylenediamine [TMPD, 0.5 mM] + ascorbate (Asc) [2.0 mM]) and sodium azide [100.0 mM]); complex V (ADP). Furthermore, the addition of the substrates cytochrome c (Cyt c) [10 μM], octanoylcarnitine (Oct) [0.2 mM], and glycerophosphate (Glp) [0.2 mM] allows the evaluation of the outer mitochondrial membrane integrity, fatty acids oxidation, and Glp dehydrogenase complex, respectively.

2.9. Ketone bodies and biochemical parameters determination

A blood sample was collected from the tail vein of the rats and measured the day before sacrifices using the glucometer Freestyle-Mini (Abbot, USA). The Freestyle-Mini glucometer is capable of detecting ketone levels between 0.00 and 8.00 mmol/L. Blood ketone values that are outside the detection limits of the device will be indicated, by consensus, as these limit values. After the sacrifice of the animals, serum glucose, cholesterol, triglyceride and alanine aminotransferase levels were analysed in the University Clinical Hospital of Santiago de Compostela (ESP), using the daily routine facilities for in-patient care and employing the Dimension EXL with LM equipment (Siemens, DEU).

2.10. Protein identification by LC-MS/MS

Protein extraction, protein digestion, and phosphopeptide enrichment and protein quantification by SWATH (Sequential Window Acquisition of all Theoretical Mass Spectra) were performed as previously established by our group [33,34]. Data analysis was carried out as previously established by our group [33,34], but for the protein/peptide library, a fold-change > 1.2 or < 0.8 and $P < 0.05$ for up-regulated or down-regulated proteins was selected.

Functional and pathway analysis were evaluated using String (https://string-db.org/), applying a minimum required interaction score of PPI= 0.7 (protein protein interaction) and an FDR < 0.05. Pathway analysis was performed employing Reactome (https://reactome.org/), which applies a statistical (hypergeometric distribution) test to determine whether certain pathways are over-represented (enriched), and generate a probability score, which is corrected for FDR using the Benjamini–Hochberg method. The most enriched pathways were represented employing Reactome pathway diagrams. Statistical analyses were performed using Markerview or Scaffold software. The volcano plot was generated using GraphPad Prism 9 (GraphPad Software Inc., USA). Cellular component and reactome pathway analysis were generated using FunRich software (http://www.funrich.org/) for data-independent acquisition analysis.

The mass spectrometry proteomics data have been deposited to the ProteomeXchange Consortium via the PRIDE [35] partner repository with the dataset identifier PXD066408, while the phosphoproteomics data are available under the separate dataset identifier PXD066410.

2.11. Metabolic profiling of rat LV tissue

Metabolic profiling of rat LV heart tissue (n = 9–10) was carried out by OWL Metabolomics S.L. by Rubió (ESP), as described previously [36]. In short, multiple ultra-high performance liquid chromatography coupled to mass spectrometry (UHPLC-MS) platforms were used to analyse endogenous analytes in the sample. The metabolites detected were included in posterior statistical analysis to evaluate possible metabolic alterations between different groups of samples. Different combinations of organic solvents were used to extract the metabolites from the sample depending on their physicochemical properties, and four different UHPLC-MS platforms were used: (1) fatty acyls, bile acids (BA), steroids and lysoglycerophospholipids, (2) glycerolipids, cholesteryl esters (ChoE), sphingolipids and glycerophospholipids, (3) amino acids (AA), and (4) polar metabolites. Lipid nomenclature and classification follow the LIPID MAPS convention, www.lipidmaps.org.

2.12. Reverse transcription polymerase chain reaction (RT-PCR)

RNA was treated with DNase to remove genomic DNA and was extracted employing a NucleoSpin kit, following the manufacturer's instructions (Macherey-Nagel, DEU). RNA quality and quantity were determined by employing a NanoDrop 1000 spectrophotometer (Thermo Scientific, USA). For relative quantification, we carried out a reverse-transcription reaction with 1 μg of RNA utilizing the Transcriptor First Strand cDNA Synthesis Kit (Roche Diagnostics, CHE) following the manufacturer's instructions. Real-time PCR was performed employing RT^2 SYBR Green® ROX™ qPCR Mastermix and specific primers supplied by provided by Qiagen® (DEU) for rat mitochondrial calcium uptake 1 (*Micu1*) (RefSeq NM_199412.2); solute carrier family 25 member 4, adenine nucleotide translocator 1 or ADP/ATP translocase 1 (*Slc25a4* or *Ant1*) (RefSeq NM_053515.2); glyceraldehyde-3-phosphate dehydrogenase (*Gapdh*) (RefSeq NM_017008.4); and 18S ribosomal RNA (*Rn18s*) (RefSeq NR_046237.1). All these primers pairs (forward and reverse) were intron-spanning and carefully designed, optimized and validated by Qiagen® (DEU). We performed RT-PCR using the Stratagene Mx3005P Real-Time PCR System following the manufacturer's instructions (Agilent Technologies, USA).

2.13. Western blot

LV heart tissues were lysed employing a TissueLysser II (Qiagen®, DEU) and were subjected to SDS-PAGE/Western blotting as we have previously explained [37], employing a primary antibody against α-tubulin (Cell Signaling Technology, Inc, USA, #3873, Lot: 16, 1:1000) following the manufacturer instructions. Mouse anti-rabbit IgG-HRP (Santa Cruz Biotechnology, Inc, USA, sc-2357, Lot # K2823, 1:1000) and m-IgGκ BP-HRP (Santa Cruz Biotechnology, Inc, USA, sc-516102, Lot # D1123, 1:1000) were used as the secondary antibodies. Chemiluminescence was used for the visualization of protein band intensities employing Clarity Western ECL Substrate (Bio-Rad Laboratories, Inc, USA) and a ChemiDoc MP Imaging System (Bio-Rad Laboratories, Inc,

USA). Normalization of protein band intensities quantification was assessed employing glyceraldehyde-3-phosphate dehydrogenase (GAPDH) (Sigma-Aldrich, USA, G9545, Batch# 0000182457 1:1000).

2.14. Statistical analysis

Experimental data are expressed as mean ± Standard Error of the Mean (SEM) of at least 4 animals per group. The measurements for food and water consumption were performed in all the animals (n = 10), however, considering that rats were housed in pairs in the metabolic cages, there are 5 measurements per group. The statistical analysis was carried out with the software GraphPad Prism 8.0.1 (GraphPad Software Inc., USA). All statistical analyses were conducted to compare experimental group with controls. Data distributions were first assessed for normality using the Kolmogorov-Smirnov test. For normally distributed data, a One-way ANOVA was performed. Homogeneity of variances was tested using the Brown–Forsythe test. If variances were homogeneous, Tukey's HSD test was used for post hoc multiple comparisons. If variances were heterogeneous, Welch's ANOVA was applied followed by Games-Howell post hoc analysis. For non-normally distributed data, the Kruskal-Wallis H test was used, with Dunn's multiple comparisons test. When comparing groups with small sample sizes (n = 5–6), the Mann-Whitney *U* test was applied. Comparisons of categorical variables (mitochondrial cristae destruction) were performed employing the Chi-squared test with a post hoc pairwise comparison applying the Bonferroni correction using R Statistical Software (v4.1.2; R Core Team, 2021, AUT; https://cran.rproject.org/). The regulation of LV proteome was analysed by the paired Student's *t* test in the normal distribution data using Markerview software (Sciex, USA). $P < 0.05$ was considered statistically significant.

Data obtained from metabolomic analysis were pre-processed using the TargetLynx application manager for MassLynx 4.1 (Waters Corporation, Massachusetts, USA). Intrabatch (multiple internal standard response correction) and interbatch (variable specific interbatch single point external calibration using repeat extracts of a commercial serum sample) normalization followed the protocol detailed in Martínez-Arranz et al., 2015 [38]. Metabolomic data are expressed as mean ± SEM and significance was established as $P < 0.05$. The statistical software package R Statistical Software (v.3.1; R Core Team, 2011, AUT; https://cran.rproject.org/) was used for the statistical analysis. Differences between obese vericiguat group and obese and lean control groups were analysed using the Student's *t*-test or Wilcoxon-Mann Whitney test.

The variation in sample sizes (n values) across analyses is attributable to the availability of cardiac left ventricle tissue, due to the diverse techniques employed in this study.

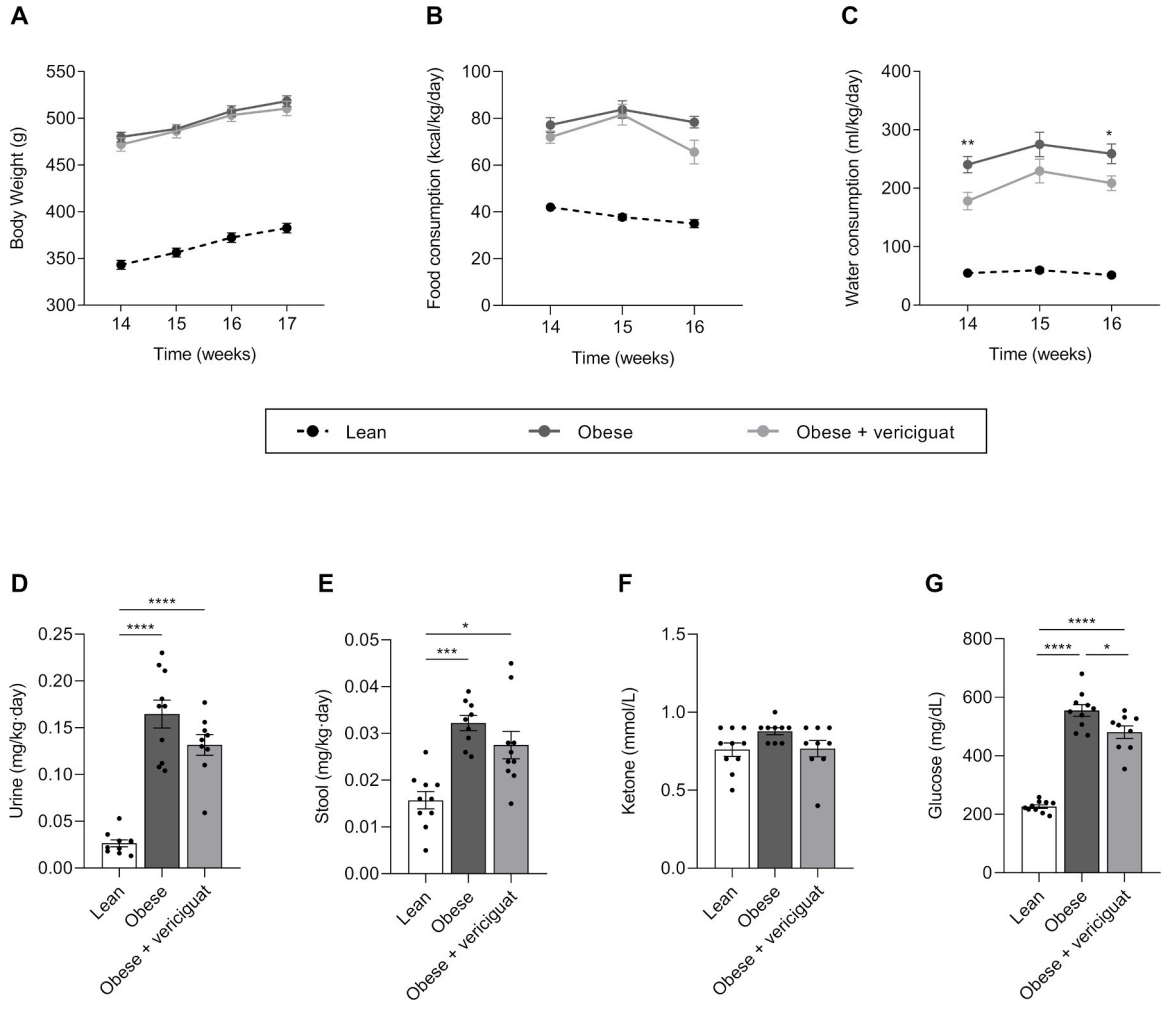

Fig. 1. Body weight, metabolic parameters and ketone and glucose levels in ZSF1 rats after treatment with vericiguat. (A) Body weight (n = 10). (B) Food consumption (n = 5, 2 animals per cage). (C) Water consumption (n = 5, 2 animals per cage). (D) Urine and (E) stool produced in 24 h (in the metabolic cages), respectively. (F) Blood ketone levels before sacrifice (n = 9–10). (G) Serum glucose levels after sacrifice (n = 9–10). Values are expressed as mean ± SEM. Comparisons between groups were performed by one-way ANOVA or Kruskal-Wallis H test. *$P < 0.05$; **$P < 0.01$; ***$P < 0.001$; ****$P < 0.0001$.

3. Results

3.1. Vericiguat effects on body weight and metabolic parameters in ZSF1 rats

Body weight, food and water consumption, and urine and stool production were significantly higher in obese ZSF1 rats compared to the lean ZSF1 control rats (Fig. 1A, B, C, D and E). Four-week treatment with vericiguat did not modify the body weight of obese vericiguat group compared to obese control group (Fig. 1A), but it reduced food consumption after two weeks of treatment (Fig. 1B), as well as water intake during the treatment (Fig. 1C). However, vericiguat did not modify the amount of urine (Fig. 1D) and stool (Fig. 1E) excreted by obese vericiguat group compared to the obese control group.

At the end of the study, blood ketone and serum glucose levels were analysed in all groups. Vericiguat treatment slightly decreased blood ketone levels in obese vericiguat group towards the values observed in the lean control group, although this result was not significant (Fig. 1F). In addition, vericiguat treatment significantly decreased glucose serum levels compared to the obese control group (Fig. 1G). Serum cholesterol, triglycerides and the liver enzyme alanine aminotransferase levels were not altered by vericiguat (data not shown). Vericiguat did not cause changes in the weight of the heart, liver, lungs, kidneys, pancreas, spleen, perirenal and perigonadal fat and gastrocnemius in ZSF1 rats (Table 1).

3.2. Vericiguat treatment ameliorates LV diastolic dysfunction

With the progress of HFpEF, IVRT values of obese control and lean control groups increased due to further deterioration of diastolic function, and obese control group had significantly increased IVRT values compared to lean control group at 17 weeks of age (Fig. 2A, Table 2). Treatment with vericiguat for three weeks improved diastolic function (IVRT) of the ZSF1 obese vericiguat group compared with the obese control group at 17 weeks of age (Fig. 2A, Table 2) but did not modify other echocardiographic parameters (Table 2) like ejection fraction (EF) (Fig. 2B), fractional shortening (FS) (Fig. 2C) and E/e' (Fig. 2D) in obese vericiguat group.

Table 1
Morphometric parameters of ZSF1 rats after vericiguat treatment. Measurements of organ weights normalized by the tibia length (TL) of ZSF1 rats after 4 weeks of vericiguat treatment. Values are expressed as mean ± SEM. (n = 9–10). Comparisons between groups were performed by one-way ANOVA or Kruskal-Wallis H test. Lean control group *vs.* obese control group: $^{\#\#\#}P < 0.001$; $^{\#\#\#\#}P < 0.0001$. Lean control group *vs.* obese vericiguat group: $^{\&}P < 0.05$; $^{\&\&}P < 0.01$ $^{\&\&\&}P < 0.001$; $^{\&\&\&\&}P < 0.0001$.

	Morphometric parameters		
	Lean group	Obese group	Obese + vericiguat group
Body weight (g)	384.60 ± 5.26$^{\#\#\#\#,\&\&\&\&}$	522.30 ± 5.07	519.00 ± 8.24
Tibia Length (mm)	39.88 ± 0.19$^{\#\#\#\#,\&\&\&\&}$	37.62 ± 0.21	37.23 ± 0.20
Heart weight (mg/mm)	29.35 ± 0.40$^{\#\#\#\#,\&\&\&\&}$	35.49 ± 0.72	34.42 ± 0.64
Liver weight (mg/mm)	282.20 ± 6.99$^{\#\#\#,\&\&\&}$	862.00 ± 18.28	855.80 ± 21.21
Lungs weight (mg/mm)	31.76 ± 0.30	33.41 ± 0.83	33.35 ± 0.85
Kidneys weight (mg/mm)	64.09 ± 2.88$^{\#\#\#\#,\&\&}$	99.62 ± 1.63	95.09 ± 2.70
Pancreas weight (mg/mm)	19.77 ± 1.46$^{\&}$	20.25 ± 1.33	23.19 ± 1.14
Spleen weight (mg/mm)	14.30 ± 0.20$^{\#\#\#\#,\&\&\&\&}$	18.68 ± 0.43	19.27 ± 0.64
Total perirenal fat weight (mg/mm)	97.48 ± 11.28$^{\#\#\#,\&\&\&}$	578.6 ± 11.99	578.2 ± 12.26
Total perigonadal fat weight (mg/mm)	102.20 ± 4.38$^{\#\#\#\#,\&\&\&\&}$	324.20 ± 9.40	321.30 ± 3.17
Gastrocnemius weight (mg/mm)	46.81 ± 0.87$^{\#\#\#,\&\&\&}$	36.91 ± 0.52	37.24 ± 1.12

3.3. Vericiguat decreases LV hypertrophy and fibrosis in ZSF1 rats

The histological analysis performed showed a significant decrease in the area of LV cardiomyocytes in the obese vericiguat group compared to the obese control group (Fig. 3A and C). Moreover, vericiguat administration significantly reduced the percentage of fibrosis (Fig. 3B and C), as well as the α-tubulin protein expression (Fig. 3D and E), in LV tissue from ZSF1 rats when compared to the obese control group.

3.4. Effect of vericiguat treatment on cardiac mitochondria respiration of ZSF1 rats

Stimulation of complex I by glutamate (once uncoupling has occurred) significantly increased the specific flux of the obese vericiguat group compared to the obese control group (Fig. 4A and B). The stimulation of β-oxidation by adding octanoylcarnitine significantly increased mitochondrial respiration in the obese vericiguat group when compared to the obese control group (Fig. 4A and B). The action of glycerophosphate produced a significant increase in the specific flux in the lean control group *vs.* the obese control group and, although the increase in mitochondrial respiration in the obese vericiguat group was not statistically significant, the levels achieved were similar to those observed in the lean control group (Fig. 4A and B), suggesting a normalization of mitochondrial respiration after vericiguat treatment.

3.5. Vericiguat partially restored the marked ultrastructural abnormalities in LV mitochondria from ZSF1 rats

Lean control group showed a preserved cytoarchitectonic structure of LV cardiomyocytes, with regularly and continuous myofibrils that alternate with serially arranged mitochondria (Fig. 5A). In the obese animals, there were marked evidence of disruption in the mitochondrial ultrastructure with mitochondrial damage, fragmentation and presence of swollen mitochondria with a more electron lucent matrix (Fig. 5B). Remarkably, these mitochondria from obese control group presented conformational changes in mitochondrial cristae morphology with cristae disarrangement, dissolution and loss (Fig. 5B), partially reverted by the treatment with vericiguat (Fig. 5C). In lean control group, the inner mitochondrial membrane (IMM) and the outer mitochondrial membrane (OMM) remain intact with a compact border (Fig. 5A), while obese animals present dissolution and rupture of IMM and/or OMM (Fig. 5B). In these obese ZSF1 rats, vericiguat can partially restore the integrity of the mitochondrial membrane (Fig. 5C).

3.6. Vericiguat preserved cristae morphology in LV mitochondria of ZSF1 rats

The analysis of mitochondrial ultrastructure by electron microscopy showed a huge heterogeneity in mitochondrial cristae disintegration (Fig. 5A, B and C), which was quantified by classifying and scoring mitochondria into three categories (Fig. 5D and E) as follows: absence of cristae destruction (absent), less than half of the mitochondria with cristae destruction (mild), and more than half of the mitochondria with cristae destruction (moderate/severe). We observed significant differences in the percentage of mitochondrial cristae destruction between the three experimental groups ($P < 0.0001$, χ^2: 54.724 for lean control group *vs.* obese control group; $P < 0.0001$, χ^2: 21.736 for lean control group *vs.* obese vericiguat group; and $P < 0.0001$, χ^2: 23.263 for obese control group *vs.* obese vericiguat group) (Fig. 5E). Obese animals presented a 90 % moderate/severe mitochondrial cristae destruction, while a 47 % and a 65 % were determined in lean control group and obese

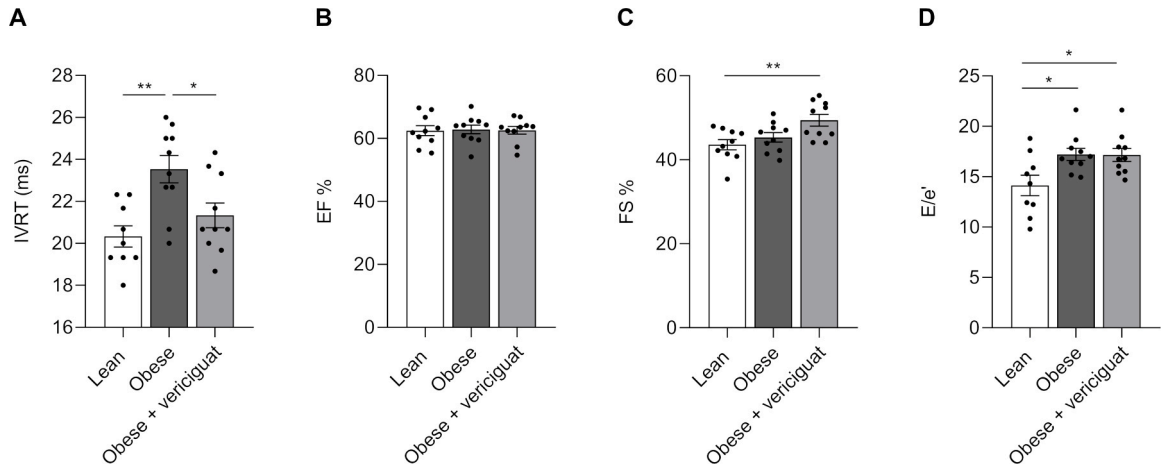

Fig. 2. Effect of vericiguat treatment on cardiac functional parameters in ZSF1 rats. (A) Isovolumic relaxation time (IVRT) (n = 9–10). (B) Ejection fraction (EF) (n = 10). (C) Fractional shortening (FS) (n = 10). (D) E/e' (n = 9–10). Values are expressed as mean ± SEM. Comparisons between groups were performed by one-way ANOVA or Kruskal-Wallis H test. $^{*}P < 0.05$; $^{**}P < 0.01$. E: early diastolic transmitral flow velocity; e': peak early-diastolic annular velocity.

Table 2
Effects of vericiguat treatment on different echocardiographic parameters in ZSF1 rats. Measurement of the echocardiographic parameters ejection fraction (EF), fractional shortening (FS), isovolumic relaxation time (IVRT), cardiac output (CO), tricuspid annular plane systolic excursion (TAPSE), E/e', E/A, left atrium area (LAA), heart rate (HR) at the end of the vericiguat treatment in ZSF1 rats. Data is expressed as mean ± SEM (n = 7–10). Lean control group *vs.* obese control group: $^{\#}P < 0.05$; $^{\#\#}P < 0.01$; $^{\#\#\#\#}P < 0.0001$. Lean control group *vs.* obese vericiguat group: $^{\&}P < 0.05$; $^{\&\&}P < 0.01$; $^{\&\&\&}P < 0.001$. Obese control group *vs.* obese vericiguat group: $^{*}P < 0.05$. Comparisons between groups were performed by one-way ANOVA or Kruskal-Wallis H test. A: late diastolic transmitral flow velocity. E: early diastolic transmitral flow velocity; e': peak early-diastolic annular velocity.

	Echocardiographic parameters		
	Lean group	Obese group	Obese + vericiguat group
% EF	62.45 ± 1.56	62.85 ± 1.38	62.59 ± 1.23
% FS	43.61 ± 1.22$^{\&\&}$	45.33 ± 1.12	49.44 ± 1.39
IVRT (ms)	20.33 ± 0.51$^{\#\#}$	23.53 ± 0.65	21.34 ± 0.59*
CO (mL·min^{-1})	109.90 ± 3.86	109.20 ± 3.73	105.50 ± 3.31
TAPSE (cm)	2.13 ± 0.13$^{\#,\&}$	2.55 ± 0.10	2.52 ± 0.08
E/e'	14.13 ± 1.02$^{\#,\&}$	17.22 ± 0.61	17.16 ± 0.65
E/A	1.875 ± 0.13	1.70 ± 0.05	1.72 ± 0.05
LAA (cm^2)	0.25 ± 0.01$^{\&}$	0.28 ± 0.01	0.28 ± 0.01
HR (min^{-1})	338.00 ± 10.09$^{\#\#\#\#,\&\&\&}$	284.90 ± 4.01	289.50 ± 4.71

vericiguat group, respectively (Fig. 5E). Remarkably, as observed in Fig. 5E, the treatment with vericiguat partially restored the mitochondrial cristae destruction of the obese animals towards the lean condition. In fact, the obese vericiguat group showed a 3 % absent, 32 % mild, and 65 % moderate/severe mitochondrial cristae destruction, while lean control group presented a 20 % absent, 32 % mild and 47 % moderate/severe destruction.

3.7. Proteomic quantitative (DIA) and qualitative (DDA) analysis in LV from ZSF1 rats

Quantitative proteomic analysis comparing the obese vericiguat group *vs.* obese control group identified 88 proteins with significantly altered expression levels. From these, we selected 22 proteins (Table 3, Supplementary Table 1) associated with the cytoskeleton, mitochondria, and the respiratory electron transport chain, based on cellular component and reactome pathway enrichment analysis (FunRich software).

Given our observation that vericiguat treatment exerts an anti-hypertrophic effect on the cardiac left ventricle tissue, we focused on a subset of cytoskeleton-related proteins. Specifically, microtubule-associated protein 4 (MAP4), tropomodulin-1 (TMOD1), and tubulin beta-4B chain (TBB4B) were downregulated in the obese vericiguat group compared to the obese control group (Table 3), whereas their expression was increased in the obese control group *vs.* lean control group (Supplementary Table 1). In addition, tropomyosin alpha-1 chain (TPM1) was also downregulated in the obese vericiguat group compared to the obese control group (Fig. 6A, Table 3).

We also observed the effect of vericiguat treatment on cardiac mitochondrial respiration proteins (Table 3, Fig. 6A). Most of the electron transport chain proteins were up-regulated in the obese vericiguat group compared with the obese control group, while the expression was sustained between the obese *vs.* lean control group (NADH dehydrogenase [ubiquinone] flavoprotein 2, mitochondrial (NDUV2), NADH dehydrogenase [ubiquinone] 1 alpha subcomplex subunit 9, mitochondrial (NDUA9), NADH dehydrogenase [ubiquinone] 1 alpha subcomplex subunit 10, mitochondrial (NDUAA), NADH-ubiquinone oxidoreductase 75 kDa subunit, mitochondrial (NDUS1), NADH dehydrogenase [ubiquinone] 1 alpha subcomplex subunit 11 (NDUAB), succinate dehydrogenase [ubiquinone] flavoprotein subunit, mitochondrial (SDHA), cytochrome b5 type B (CYB5B), ATP synthase subunit gamma, mitochondrial (ATPG) and ATP synthase F(0) complex subunit B1, mitochondrial (AT5F1), ADP/ATP translocase 1 (ADT1)). Other proteins associated with protection against oxidative stress were up-regulated in the obese vericiguat group compared with the obese control group, while the expression was downregulated or sustained between the obese *vs.* lean control group (thioredoxin-dependent peroxide reductase, mitochondrial (PRDX3), peroxiredoxin-5, mitochondrial (PRDX5), peroxiredoxin-6 (PRDX6), superoxide dismutase [Mn], mitochondrial (SODM), voltage-dependent anion-selective channel protein 3 (VDAC3), ES1 protein homolog, mitochondrial (ES1)) (Table 3, Fig. 6A and B). AT5F1, PRDX5 and PRDX6 proteins are slightly below the selected fold-change threshold (fold-change >1.2) but, as they form clusters with other proteins mentioned above, they have been selected. Two proteins associated with tricarboxylic acid cycle (isocitrate dehydrogenase [NAD] subunit gamma 1, mitochondrial (IDHG1), malate dehydrogenase, mitochondrial (MDHM)), had their expression increased in the obese vericiguat group compared with the obese control group: the first one had its expression sustained between the obese *vs.* lean control

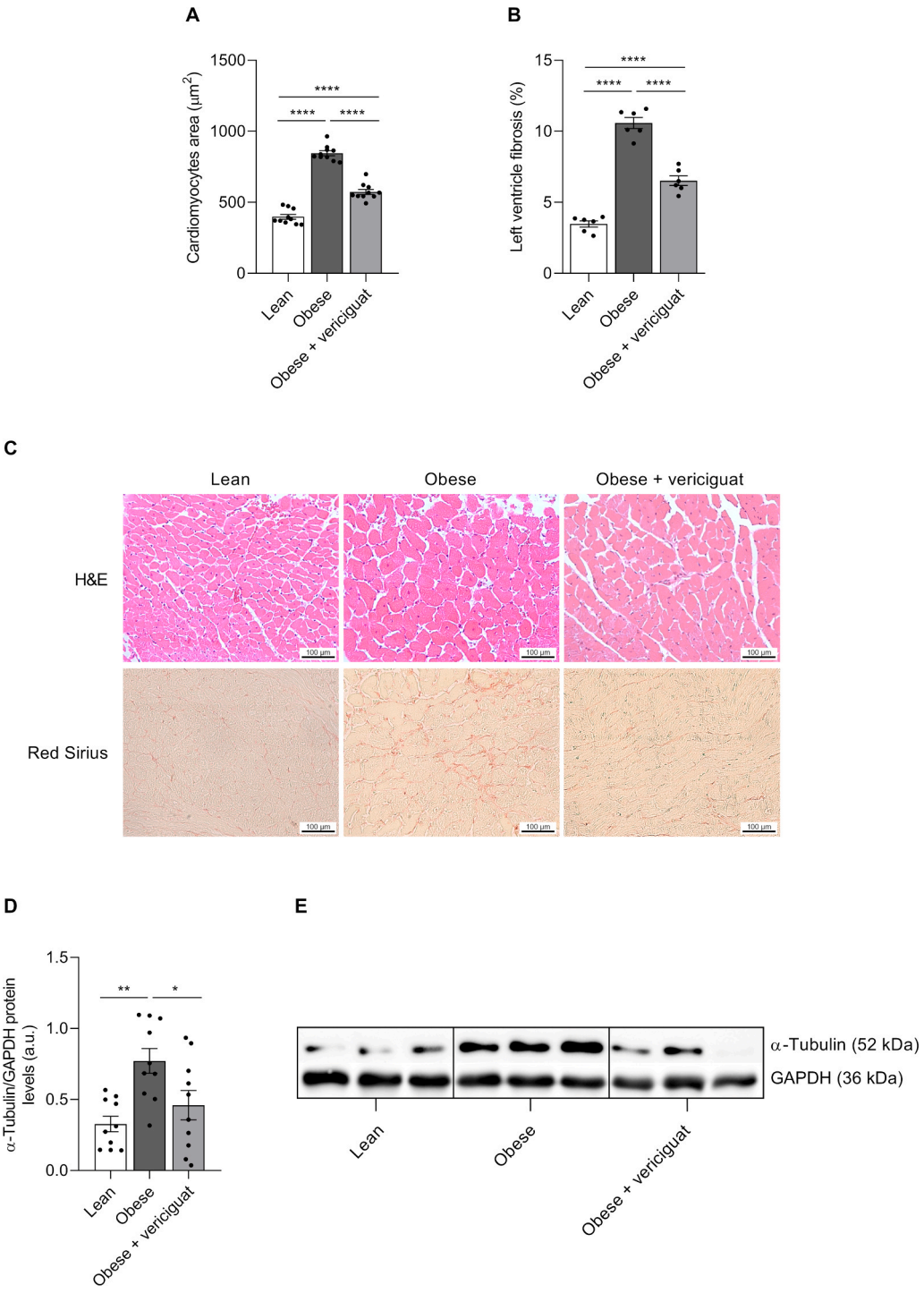

Fig. 3. Effect of vericiguat on hypertrophy, fibrosis and protein levels of α-tubulin in LV tissues from ZSF1 rats. (A) Quantitative analysis of myocardial hypertrophy based on cardiomyocyte area on LV tissue of ZSF1 rats treated with vericiguat compared to obese and lean control animals (n = 10). (B) Quantitative analysis of the percentage of fibrosis on LV tissue of ZSF1 rats treated with vericiguat compared to obese and lean control animals (n = 6). (C) Representative histological images from LV cardiomyocytes stained with H&E in each group of animals (magnification of X40) and with Picro-sirius red in each group of animals (magnification x20). (D) Statistical analysis of α-tubulin protein expression levels in LV tissues of ZSF1 rats treated with vericiguat when compared to obese and lean control animals (n = 10). (E) Representative photographs showing α-tubulin protein expression levels in LV tissues of ZSF1 rats. Values are expressed as mean ± SEM. Comparisons between groups were performed by one-way ANOVA or Kruskal-Wallis H test. *$P < 0.05$; **$P < 0.01$; ****$P < 0.0001$. LV: left ventricle. Scale bar: 100 μm.

groups, while the last one had its expression downregulated between the obese *vs.* lean control groups (Table 3, Fig. 6A and B).

Qualitative proteomic analysis enabled us to identify proteins present in each particular group. Among those present both in the lean control group and the obese vericiguat group, and absent in the obese control group, we identified a protein involved in the recognition and mediation of the translocation of mitochondrial preproteins from the cytosol into the mitochondria (mitochondrial import receptor subunit TOM70 (TOM70)) (Fig. 6B).

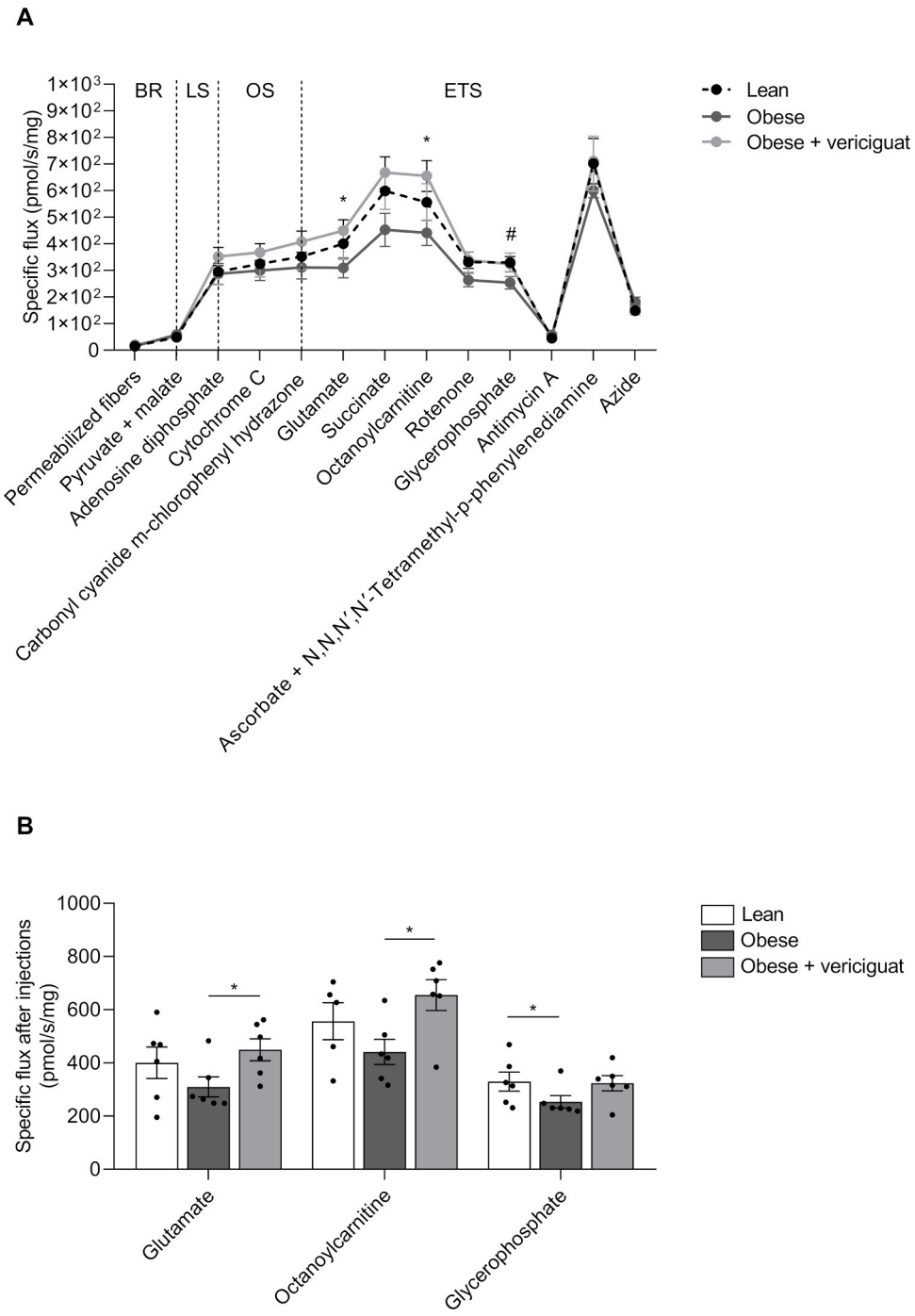

Fig. 4. Mitochondria respiration in the LV of ZSF1 rats after vericiguat treatment. (A) Graphical representation of the effect of vericiguat treatment on mitochondrial basal respiration of permeabilised LV fibres and after the addition of different substrates (pyruvate+malate, adenosine diphosphate, cytochrome c, glutamate, succinate, octanoylcarnitine and ascorbate and N,N,N′,N′-Tetramethyl-p-phenylenediamine), an uncoupler (carbonyl cyanide m-chlorophenyl hydrazone) and inhibitors (rotenone, glycerophosphate, antimycin A and azide) (n = 6). (B) Effects on mitochondria respiration after addition of glutamate, after the stimulation of β-oxidation by adding octanoylcarnitine and after addition of glycerophosphate (n = 5–6). Values are expressed as mean ± SEM. Comparisons between groups were performed by Mann-Whitney *U* test. Obese vericiguat group *vs.* obese control group $^{*}P < 0.05$; obese control group *vs.* lean control group $^{\#}P < 0.05$. BR: basal respiration, ETS: electron transfer state, LS: LEAK state, LV: left ventricle, OS: OXPHOS state.

3.8. Phosphoproteomic analysis in LV from ZSF1 rats

Quantitative proteomic analysis comparing the obese vericiguat group with the obese control group identified 49 phosphorylated proteins with significantly altered levels. From these, we selected 3 proteins related to mitochondrial function, specifically the Krebs cycle, the malate-aspartate shuttle and the mitochondrial translation machinery. Vericiguat treatment increased the phosphorylation of aspartate aminotransferase, mitochondrial (AATM), and malate dehydrogenase, mitochondrial (MDHM). Conversely, vericiguat decreased the phosphorylation of elongation factor Tu, mitochondrial (EF-TU_{mt}) (Fig. 6B). Additionally, we selected 2 phosphorylated proteins involved in the pentose phosphate pathway (PPP), 6-phosphogluconolactonase (6PGL) and 6-phosphogluconate dehydrogenase, decarboxylating (6PGD), which were increased in the obese vericiguat group (Table 3, Supplementary Table 1).

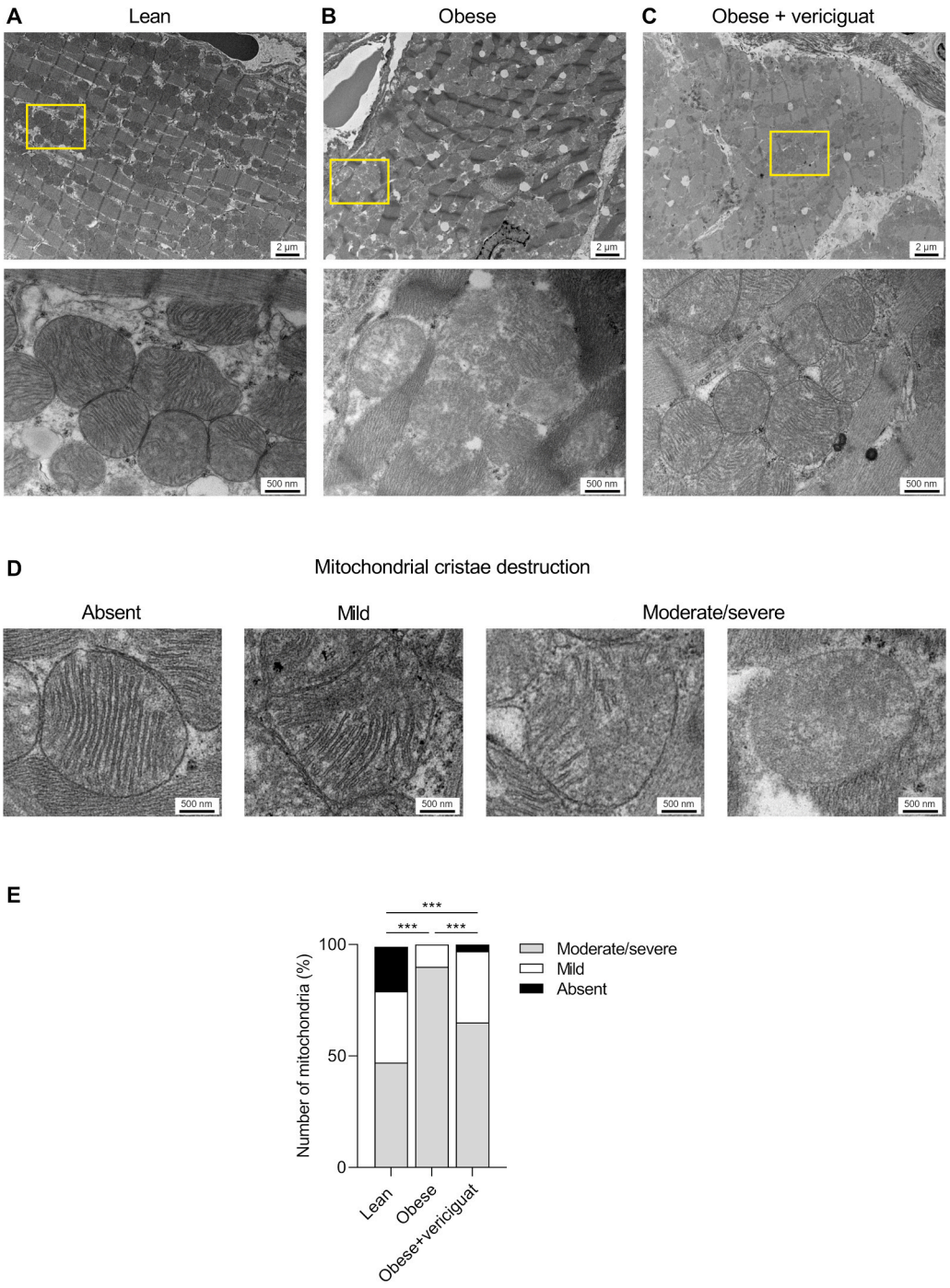

Fig. 5. LV electron micrographs of mitochondrial ultrastructural morphological characteristics and mitochondrial cristae destruction. Representative electron micrographs showing cardiac mitochondria localized in the LV of lean control group (A), obese control group (B) and obese vericiguat group (C) at a low magnification of x5000 (first row) and a high magnification of x30000 (second row). Representative electron microscopy images of mitochondrial cristae in different stages of disintegration (D). Qualitative analysis of electron micrographs features for mitochondrial cristae destruction (E) scored as absent, mild and moderate/severe showed significant differences between the three experimental groups ($P < 0.0001$, χ^2: 54.724 for lean control group *vs.* obese control group; $P < 0.0001$, χ^2: 21.736 for lean control group *vs.* obese vericiguat group; and $P < 0.0001$, χ^2: 23.263 for obese control group *vs.* obese vericiguat group). A total of 125–148 mitochondria were analysed from 4 LV samples of each group. The scale bar corresponds to 2 µm in the micrographs of the first row and 500 nm in the micrographs of the second row. Values are expressed as percentages. Comparisons between groups were performed by Chi-squared test with a post hoc pairwise comparison applying the Bonferroni correction. LV: left ventricle.

3.9. Vericiguat modulates the mRNA levels of mitochondrial membrane proteins in ZSF1 rats

Vericiguat treatment significantly reduced the gene expression levels of the Ca^{2+}-sensing regulator *Micu1* of the mitochondrial Ca^{2+} uniporter complex in rat LV when compared to the obese rats (Fig. 7A). Moreover, the obese vericiguat group showed a significant increase in the cardiac mRNA levels of the master regulator of mitochondrial energy output, the ADP/ATP translocase 1 (*Slc25a4* or *Ant1*), when compared to the obese control group (Fig. 7B).

Table 3
Proteomic and phosphoproteomic analysis of LV tissue from ZSF1 rats after treatment with vericiguat. Table showing the differential protein expression between the augmented proteins in the obese vericiguat group (positive log_2 (fold-change) in green) *vs.* those augmented in the obese control group (negative log_2 (fold-change) in red) (n = 10, $P < 0.05$) from those 22 proteins that we have selected associated with cytoskeleton, mitochondria (electron transport chain and tricarboxylic acid cycle) and the protection against oxidative stress. LV: left ventricle.

			Obese + vericiguat group *vs.* Obese group		
Uniprot	Protein	Protein name	*P value*	Fold-change	log_2 (fold-change)
		Cytoskeleton			
Q5M7W5	**MAP4**	Microtubule-associated protein 4	0.000	0.736	−0.442
P70567	**TMOD1**	Tropomodulin−1	0.020	0.785	−0.350
P04692	**TPM1**	Tropomyosin alpha−1 chain	0.011	0.793	−0.334
Q6P9T8	**TBB4B**	Tubulin beta−4B chain	0.016	0.800	−0.321
		Electron transport chain			
P19511	**AT5F1**	ATP synthase F(0) complex subunit B1, mitochondrial	0.039	1.192	0.253
Q920L2	**SDHA**	Succinate dehydrogenase [ubiquinone] flavoprotein subunit, mitochondrial	0.013	1.232	0.301
Q561S0	**NDUAA**	NADH dehydrogenase [ubiquinone] 1 alpha subcomplex subunit 10, mitochondrial	0.007	1.282	0.359
Q66HF1	**NDUS1**	NADH-ubiquinone oxidoreductase 75 kDa subunit, mitochondrial	0.012	1.347	0.430
P19234	**NDUV2**	NADH dehydrogenase [ubiquinone] flavoprotein 2, mitochondrial	0.000	1.410	0.496
Q80W89	**NDUAB**	NADH dehydrogenase [ubiquinone] 1 alpha subcomplex subunit 11	0.043	1.571	0.652
P35435	**ATPG**	ATP synthase subunit gamma, mitochondrial	0.003	1.574	0.654
P04166	**CYB5B**	Cytochrome b5 type B	0.009	1.662	0.733
Q5BK63	**NDUA9**	NADH dehydrogenase [ubiquinone] 1 alpha subcomplex subunit 9, mitochondrial	0.001	1.672	0.742
Q05962	**ADT1**	ADP/ATP translocase 1	0.005	1.870	0.903
		Protection against oxidative stress			
Q9R063–2	**PRDX5**	Isoform cytoplasmic + peroxisomal of Peroxiredoxin−5, mitochondrial	0.021	1.170	0.227
O35244	**PRDX6**	Peroxiredoxin−6	0.007	1.182	0.241
Q9Z0V6	**PRDX3**	Thioredoxin-dependent peroxide reductase, mitochondrial	0.014	1.255	0.328
P07895	**SODM**	Superoxide dismutase [Mn], mitochondrial	0.010	1.291	0.368
P56571	**ES1**	ES1 protein homolog, mitochondrial	0.010	1.354	0.437
Q9R1Z0	**VDAC3**	Voltage-dependent anion-selective channel protein 3	0.043	1.384	0.469
		Tricarboxylic acid cycle			
P41565	**IDHG1**	Isocitrate dehydrogenase [NAD] subunit gamma 1, mitochondrial	0.018	2.007	1.005
P04636	**MDHM**	Malate dehydrogenase, mitochondrial	0.029	1.271	0.346
		Phosphoproteins (phosphorylation levels)			
P85971	**6PGL**	6-Phosphogluconolactonase	0.027	2.717	1.442
P85968	**6PGD**	6-Phosphogluconate dehydrogenase, decarboxylating	0.021	2.382	1.252
P04636	**MDHM**	Malate dehydrogenase, mitochondrial	0.018	2.066	1.047
P00507	**AATM**	Aspartate aminotransferase, mitochondrial	0.044	1.385	0.470
P85834	**EFTU**	Elongation factor Tu, mitochondrial	0.033	0.377	−1.407

3.10. Vericiguat treatment modulates several metabolites in LV tissue from ZSF1 rats

A total of 396 metabolic features were detected in the analysed rat heart tissue samples using untargeted metabolomics. Few differences between metabolites from obese control and obese vericiguat groups were found in the untargeted metabolomic analysis of cardiac tissues, with six (6) metabolites (arginine, S-adenosyl-homocysteine, sphingomyelin 42:1, ether-linked phosphatidylethanolamines P-18:0/18:1, phosphatidylcholine 40:7 and the ratio phosphatidylcholine/phosphatidylethanolamine) reaching a significance threshold ($P < 0.05$). Between all those six metabolites, arginine has been reported to be the most closely linked to cardiac performance and outcomes, especially in heart failure with preserved ejection fraction [39].

Since metabolites significantly altered in the comparison between obese and lean control groups, but not in the comparison between obese vericiguat *vs*. obese control rats, are also indicative of the effectiveness of the drug, we decided to select the most relevant changes of that comparison. Among metabolites fulfilling this condition, we considered remarkable the upregulation in the obese vericiguat group of the decreased levels of 6-phosphogluconate and D-ribose 5-phosphate observed in the obese control group, since both are critical metabolites of the PPP, which has been tightly associated with potential metabolic disturbances, heart failure, type 2 diabetes mellitus and their complications [40].

In summary, cardiac arginine, D-ribose 5-phosphate and 6-phosphogluconate levels were found to be significantly dropped in obese animals compared to lean controls (Fig. 8). Vericiguat treatment partially restored the arginine levels (Fig. 8A) and prevented the decrease of D-ribose 5-phosphate (Figs. 8B) and 6-phosphogluconate (Fig. 8C) observed in the obese control group.

4. Discussion

Major obstacles limiting the development of effective strategies to improve clinical outcomes in chronic HF, particularly in HFpEF patients, include the considerable heterogeneity of the HFpEF spectrum, the failure to identify patient subgroups likely to benefit, and, importantly, the need for earlier therapeutic interventions [41–43]. It is generally recognised that early detection and intervention will help to halt the progression of HFpEF, to prolong healthy life expectancy, and to ameliorate quality of life [43–46].

The diversity of HFpEF comorbidities, the complex pathophysiological molecular mechanisms, and the resultant altered signalling pathways are major factors promoting the development of HFpEF pathologies [44–47]. The design of more personalized treatments, with combinations of drugs that interfere with different molecular pathways, may help to improve the prognosis and prolong the survival time of HFpEF patients [47–50]. One of the major signalling cascades for the regulation of cardiovascular function is the NO–soluble GC (sGC)–cGMP pathway, whose suppression is tightly involved in the progression of HFrEF and HFpEF, being, at least partly, the cause of cardiac dysfunction in chronic heart failure [47,51,52]. Inhibition and impairment of NO–sGC–cGMP pathway have been observed in clinical patient samples

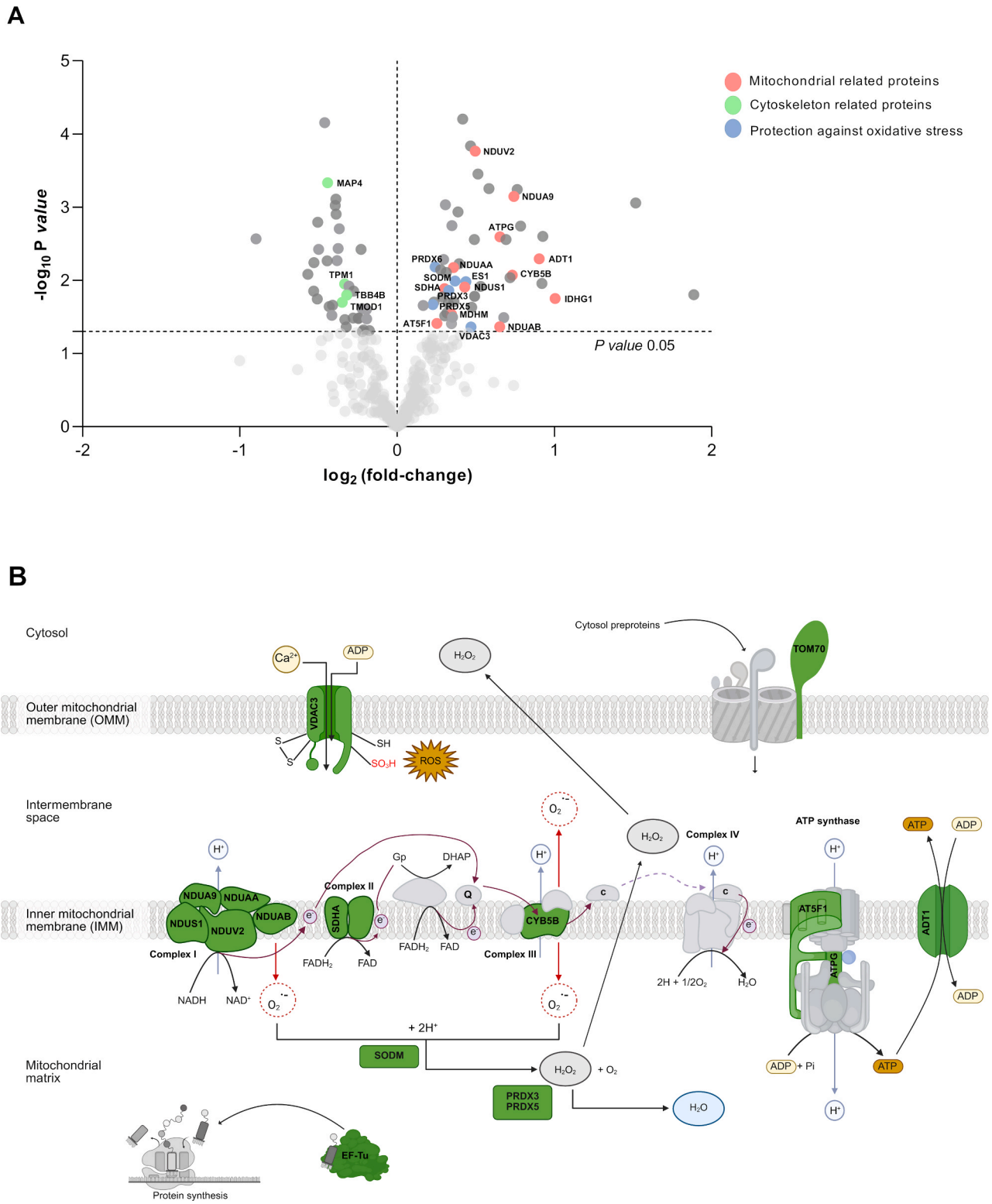

Fig. 6. Proteomic and phosphoproteomic analysis of LV tissue from ZSF1 rats after treatment with vericiguat. (A) Volcano plot showing the differential protein expression between the obese control group (left) compared to the obese vericiguat group (right) (n = 10). (B) Representative illustration of the enhanced proteins of the electron transport chain and others correlated to mitochondria in the obese vericiguat group. Created in https://BioRender.com. LV: left ventricle. ADT1: ADP/ATP translocase 1, AT5F1: ATP synthase F(0) complex subunit B1, ATPG: ATP synthase subunit gamma, CYB5B: cytochrome b5 type B, EF-Tu: elongation factor Tu, NDUA9: NADH dehydrogenase [ubiquinone] 1 alpha subcomplex subunit 9, NDUAA: NADH dehydrogenase [ubiquinone] 1 alpha subcomplex subunit 10, NDUAB: NADH dehydrogenase [ubiquinone] 1 alpha subcomplex subunit 11, NDUS1: NADH-ubiquinone oxidoreductase 75 kDa subunit, NDUV2: NADH dehydrogenase [ubiquinone] flavoprotein 2, PRDX3: thioredoxin-dependent peroxide reductase, PRDX5: isoform cytoplasmic + peroxisomal of Peroxiredoxin-5, SDHA: succinate dehydrogenase [ubiquinone] flavoprotein subunit, SODM: superoxide dismutase [Mn], TOM70: mitochondrial import receptor subunit TOM70, VDAC3: voltage-dependent anion-selective channel protein 3.

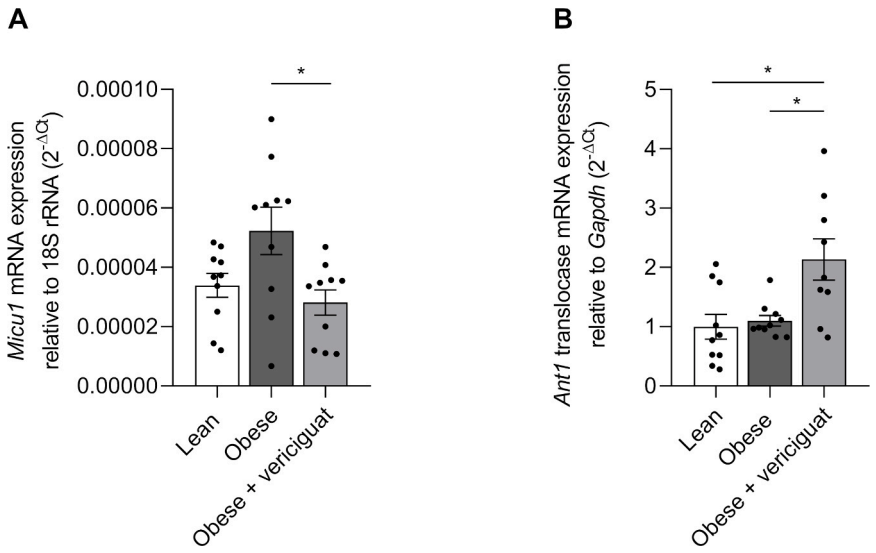

Fig. 7. Effect of vericiguat on gene expression of mitochondrial membrane proteins in LV tissue. (A) RT-PCR for *Micu1* (n = 10). (B) RT-PCR for *Ant1* (n = 9–10). Values are expressed as mean ± SEM. Comparisons between groups were performed by one-way ANOVA or Kruskal-Wallis H test. *$P < 0.05$. *Micu1*: mitochondrial calcium uptake 1. *Ant1*: adenine nucleotide translocator 1 or ADP/ATP translocase 1. *Gapdh*: glyceraldehyde-3-phosphate dehydrogenase. LV: left ventricle.

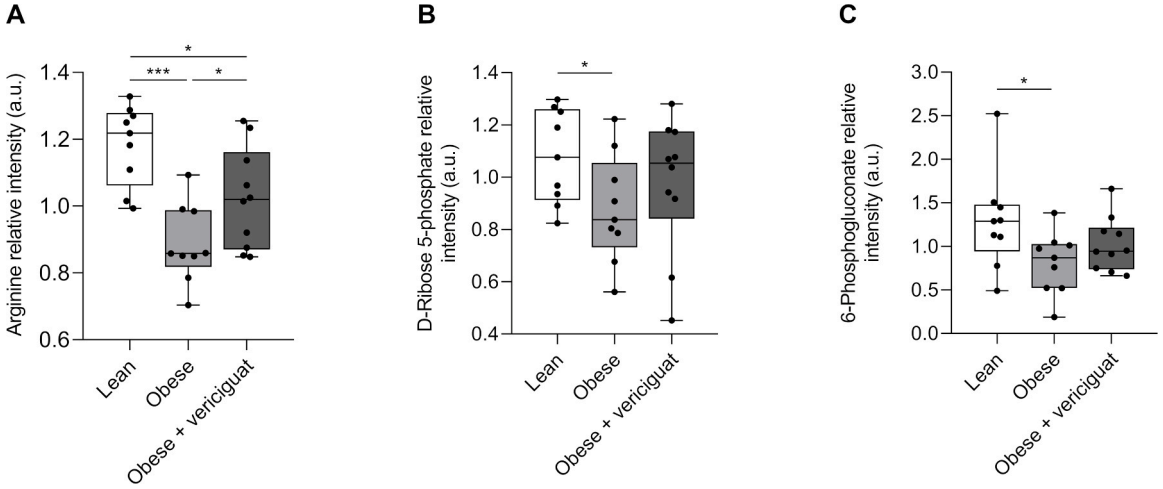

Fig. 8. Metabolomic analysis of LV tissue from ZSF1 rats treated with vericiguat. (A) Bloxplot representing the relative intensity of the amino acid arginine (n = 9–10). (B) Boxplot representing the levels of the carbohydrate derivative D-Ribose 5-phosphate (n = 9–10). (C) Bloxplot representing the relative intensity of 6-Phosphogluconate (n = 9–10). Comparisons between groups were performed by Student's *t*-test or Wilcoxon-Mann Whitney test. *$P < 0.05$; ***$P < 0.001$. a.u.: arbitrary units. LV: left ventricle.

and in a variety of experimental animal HFpEF models, which urges research to provide more targeted therapeutic strategies involving the recovery of sGC-cGMP signalling [47]. Importantly, it has been hypothesised that initiating therapy at an advanced stage of the disease may reduce the efficacy of NO-cGMP-based interventions, mainly due to irreversible microvascular and myocardial remodelling [41].

The sGC stimulator vericiguat has beneficial effects in HFrEF treatment, but it has not been proved yet to be efficacious in HFpEF based on recent trials [51]. The main novelty of our work is the demonstration, for the first time, that the treatment with a sGC stimulator (vericiguat) is able to improve diastolic dysfunction, to stimulate cardioprotective metabolic processes such as the pentose phosphate pathway (PPP), to ameliorate cardiac mitochondrial function, and to increase the cardiac levels of pivotal mitochondrial proteins involved in antioxidant processes, when it is administered in a preclinical model of early-stage HFpEF.

To study the effects of the treatment with vericiguat during the development of left ventricle diastolic dysfunction, we used the Zucker fatty /spontaneously hypertensive (ZSF1) rats. This preclinical model of cardiometabolic HFpEF presents hypertension, hyperlipidaemia, obesity, and diabetes, which are already seen at the age of 6 weeks [25,53,54]. Although all HFpEF animal models are reflecting only parts of human aetiologies and HFpEF characteristics, the ZSF1 rat model is considered a rather predictive animal model of HFpEF [51–54]. Obese ZSF1 rats develop signs of diastolic dysfunction, as deduced from echocardiographic and invasive measurements, at the age of 10–15 weeks, with a rise in BNP expression and concomitant muscle atrophy, which fulfil all criteria for diagnosis of HFpEF [54–57]. Consequently, ZSF1 rats at 14 weeks may be considered a suitable animal model to test initial intervention with new pharmacological strategies for early-stage HFpEF.

In this study, treatment with vericiguat for four weeks did not affect the body weight of ZSF1 rats or the weights of the heart, kidney, lung, liver, pancreas, spleen, perirenal and perigonadal fat, or gastrocnemius muscle. Importantly, vericiguat treatment significantly reduced serum glucose levels in our animal model of early-stage HFpEF with diabetes

and obesity. This is in line with data demonstrating a blood glucose-lowering effect of praliciguat in obese ZSF1 rats [58]. However, treatment with other sGC stimulators did not demonstrate this reduction in blood glucose levels in different animal models of metabolic disease: Reverte et al. (2022) found that fasting glucose plasma levels of hypertensive rats with prolonged exposure to high-fat diet were not modified after a treatment with the sGC stimulator praliciguat for 6 weeks [59]; while Patel et al. (2023) observed that blood glucose levels were not significantly affected by an acute treatment with the sGC stimulator BAY 41–2272 or the sGC activator runcaciguat in mice models of mild type-2 diabetes [60]. Our results suggest, however, that vericiguat may improve the diabetic phenotype, and confirm previous findings indicating that pharmacological stimulation of sGC can have beneficial metabolic effects, including additional glucose-lowering effects beyond the current standard of care [59,61,62].

Treatment of obese ZSF1 rats with vericiguat during 4 weeks (from 14 to 18 weeks of age) improved diastolic dysfunction (epicentre of HFpEF) at the end of treatment, as demonstrated by echocardiography showing a significant reduction in IVRT. Two studies have reported improvements in cardiac function in animal models of cardiovascular disease after vericiguat treatment: Jungtanasomboon et al. (2023) showed that vericiguat was able to ameliorate left ventricular dysfunction in a rat model of mitral regurgitation [63]; while Zeng et al. (2024) have recently reported that vericiguat partially reversed the doxorubicin-induced decrease in cardiac left ventricle ejection fraction and fraction shortening in a mouse model of cardiotoxicity [64]. Mira-Hernández et al. (2024) have very recently reported an improvement in cardiomyocyte electrophysiology in cultured cardiac cells from a female mouse model of HFpEF (leptin receptor-deficient *db/db* mice with aldosterone infusion for 4 weeks) [20]. However, our data provide a first evidence of a positive effect of vericiguat on cardiac function in an animal model of early-stage HFpEF.

We have demonstrated for the first time an antihypertrophic effect of vericiguat treatment on cardiac tissue in an animal model of early-stage HFpEF. Histological analysis revealed a significant reduction in the area of left ventricular cardiomyocytes following vericiguat treatment. Moreover, vericiguat administration significantly decreased the percentage of fibrosis and α-tubulin protein expression in left ventricular tissue from ZSF1 rats. Previous experimental research has suggested potential benefits of sGC stimulators in preventing, or even reversing, cardiac hypertrophy and fibrosis, proposing that impaired cGMP formation may contribute to the pathophysiology of fibrosis and hypertrophy in cardiovascular tissues [51,65,66]. Specifically, the sGC stimulator riociguat reduced right ventricular hypertrophy in specific animal models of pulmonary hypertension or right ventricular hypertrophy, although other authors found no significant effect [51,67,68]. In addition, vericiguat treatment resulted in a reduction of cardiac hypertrophy in studies with L-NAME-treated renin transgenic rats and in angiotensin II-treated mice [69,70]. In HF, cardiac hypertrophy and stiffness are linked to the microtubule, intermediate filament, and actomyosin networks' pathological remodelling [71], being many cytoskeletal-related proteins upregulated in failing hearts [72]. Proteomic analysis of cardiac tissue in our study demonstrated that, even at an early stage of HFpEF, vericiguat treatment reduces the expression of the cytoskeleton-associated proteins tubulin β-4B chain (TUBB4B), microtubule-associated protein 4 (MAP4) and tropomodulin-1 (TMOD1), which were significantly elevated in the obese control group. TUBB4B is one of the most abundant β-tubulin isoforms expressed in the heart, where it dimerises with α-tubulin to conform the microtubules [73], and has been suggested to play a relevant role in the development of hypertrophy and fibrosis, with its cardiac protein levels upregulated in human HF [73,74]. MAP4 is one of the structural microtubule-associated proteins that act as a cytoskeleton regulator, and its upregulation is associated with cardiac remodelling [75,76]. We found MAP4 levels to be increased in the hearts of obese compared with lean animals, while the treatment with vericiguat reduced this protein. TMOD1 is the isoform predominantly expressed in the heart within the tropomodulin family cytoskeletal regulatory proteins, whose overexpression has been linked to cardiac hypertrophy [77]. TMOD1 cardiac expression was significantly increased in obese compared with lean animals, but its levels decreased after the treatment with vericiguat. Likewise, vericiguat treatment reduced cardiac levels of the predominant tropomyosin isoform in the heart, TPM1, whose increased cardiac expression has been associated with impaired cardiac performance in HF [78].

Previous studies have demonstrated alterations in the quantity, structure and energy metabolism of cardiac mitochondria both in humans with HFpEF and in animal models of the disease [79]. Furthermore, cGMP is known to play a role in a variety of cellular processes, including mitochondrial biogenesis [80]. It has been proposed that cardiac mitochondria may be critical in the cardioprotection against ischemia-reperfusion injury mediated by cGMP-stimulating compounds [81,82]. In the present study, mitochondrial function and oxidative phosphorylation in cardiac tissue from ZSF1 rats treated with vericiguat were evaluated by measuring the rate of oxygen consumption in cardiac left ventricular fibres, as previously described [83]. Treatment with vericiguat induced a positive effect on mitochondrial basal respiration of permeabilised cardiac left ventricular fibres following the addition of various substrates in our animal model of early-stage HFpEF. This finding aligns with the reported improvement in mitochondrial respiratory capacity in cardiac tissue of ZSF1 rats treated with the sodium-glucose cotransporter-2 (SGLT2) inhibitor empagliflozin [55]. The enhanced mitochondrial respiration capacity observed in the obese vericiguat group could contribute to a healthier metabolic phenotype in this HFpEF animal model, likely reflecting improved mitochondrial quality. Mitochondrial integrity and function derangements, including mitochondrial cristae separation and dissolution, represent critical pathophysiological features in HFpEF pathogenesis [84]. Electron microscopy revealed a diffuse dissolution and loss of mitochondrial cristae in hearts of obese control rats, which was partially restored by vericiguat treatment.

Compared with non-failing donor hearts, the activity rates of complexes I and IV, as well as the Krebs cycle enzymes isocitrate dehydrogenase and malate dehydrogenase, have been found to be lower in human HF [85]. Krebs cycle intermediates were also found reduced in human cardiac tissue from HFpEF patients [84]. We have observed, using proteomics, that the treatment with vericiguat is able to increase the cardiac levels of the Krebs cycle enzymes isocitrate dehydrogenase and malate dehydrogenase. To note, phosphoproteomic analysis showed a significant increase in the cardiac levels of phosphorylated malate dehydrogenase and aspartate aminotransferase in the ZSF1 obese animals treated with vericiguat. In the heart, the malate-aspartate shuttle constitutes the primary metabolic pathway for the transfer of reducing equivalents from the cytosol into the mitochondria for oxidation, and it is associated with preservation of mitochondrial function and cell survival [86,87]. Many studies have provided evidence that protein phosphorylation within mitochondria is of critical importance [88]. In particular, it has been proved that the cardiac levels of phosphorylation of aspartate aminotransferase are linked to cardioprotection [89]. Myocardial proteomics has recently revealed also reductions in mitochondrial respiration proteins in obese patients with HFpEF [84]. It has been previously described that the hearts of obese ZSF1 rats have a different expression of genes implicated in mitochondrial respiration [52], a process firmly involved in the development of HFpEF [90]. Our data clearly demonstrate that vericiguat was able to upregulate the cardiac levels of mitochondrial electron transport chain proteins, including five proteins from complex I (mitochondrial NADH dehydrogenase [ubiquinone] flavoprotein 2, (NDUV2), NADH dehydrogenase [ubiquinone] 1 alpha subcomplex subunit 9 (NDUA9), NADH dehydrogenase [ubiquinone] 1 alpha subcomplex subunit 10 (NDUAA), NADH-ubiquinone oxidoreductase 75 kDa subunit (NDUS1), NADH dehydrogenase [ubiquinone] 1 alpha subcomplex subunit 11 (NDUAB),

one protein from complex II (succinate dehydrogenase [ubiquinone] flavoprotein subunit (SDHA)), and one protein from complex III (cytochrome b5 type B (CYB5B)). To note, it has been demonstrated that enhancements of cardiac mitochondrial complex I, complex II and/or complex III proteins expression and activity can reduce aberrations in mitochondrial cristae and can improve mitochondrial respiratory function in HF [91–94]. Importantly, the cardiac levels of mitochondrial subunits of the complex V (ATP synthase), subunit gamma (ATPG) and subunit B1 (AT5F1), were also significantly increased by the treatment with vericiguat. ATP synthase is an important molecular motor that catalyses the final coupling step of oxidative phosphorylation to supply energy in the form of ATP, and it is also essential in sustaining mitochondrial structure, organization and function, being its impairment associated with energy depletion in HF [95,96]. All these changes induced by vericiguat imply an improvement in mitochondrial respiratory capacity, which has been associated with beneficial effects on diastolic function in animal models of HFpEF [55]. In addition, the treatment with vericiguat increased the cardiac levels of the ADP/ATP translocase 1, that exports mitochondrial adenosine triphosphate into the cytosol and plays a key role in cardiomyocyte contraction and calcium transport, and whose deficiency results in cardiac dysfunction and HF [97–99].

The oxidation phosphorylation machinery is under an accurate dual control assembled in a highly orchestrated manner: most of its subunits are encoded by nuclear DNA, translated by cytosolic ribosomes and imported into mitochondria, while the rest are directly encoded by mitochondrial DNA [100,101]. Mitochondrial proteins synthesized on cytosolic ribosomes are imported into the mitochondria using the TOM (translocase of the outer membrane) complex as the common entry gate [102]. A key component of the TOM complex and its response to altered metabolic situations is the major import receptor TOM70 [102], that we have found upregulated by vericiguat in the cardiac tissue of ZSF1 rats. TOM70 is involved in protein import, contacts the endoplasmic reticulum and the nucleus, and is linked to the control of energy metabolism, to protection against diet-induced obesity and (in concordance with our electron microscopy results) to the control of mitochondrial cristae formation [103]. On the other hand, mitochondrial ribosomal proteins and various translational elongation factors, including Tu (EF-Tu_{mt}), are fundamental regulators of mitochondrial translation of oxidative phosphorylation subunits encoded by mitochondrial DNA [104]. The phosphoproteome of the cardiac tissue of ZSF1 rats after treatment with vericiguat showed a significant decrease in the phosphorylation of EF-Tu_{mt}. EF-Tu_{mt} phosphorylation has been reported to be able to regulate its activity [105]. Specifically, it has been suggested that the phosphorylation of EF-Tu_{mt} in the myocardium inhibits mitochondrial protein synthesis and associates with cardiac damage [106].

Mitochondrial Ca^{2+} transport is an emerging topic in HF progression, playing the fluctuations in mitochondrial matrix Ca^{2+} a critical role in adjusting energy production to cellular demand through direct effects on oxidative phosphorylation and ATP production [107]. Mitochondrial Ca^{2+} uptake occurs via the mitochondrial Ca^{2+} uniporter (MCU), that is regulated by mitochondrial uptake proteins (MICU) 1, 2, and 3 [108]. The two regulators MICU1 and MICU2, as well as the MICU1/MCU ratio, have been found elevated in the failing human heart, suggesting altered Ca^{2+}gating associated with cardiac contractile dysfunction [109]. In this work, we demonstrate that the treatment with vericiguat is able to significantly reduce the cardiac levels of MICU1.

An elevation of mitochondrial reactive oxygen species production has also been found in the cardiac tissue of animal models of HFpEF [110], and it is known that mitochondrial oxidative stress contributes to diastolic dysfunction in HF [22]. The treatment with vericiguat significantly increased the cardiac levels of several pivotal mitochondrial proteins involved in antioxidant processes, such as thioredoxin-dependent peroxide reductase (PRDX3), peroxiredoxin-5 (PRDX5), peroxiredoxin-6 (PRDX6), superoxide dismutase (SODM), voltage-dependent anion-selective channel protein 3 (VDAC3) and ES1 protein homolog (ES1) [111–116]. On the other hand, the metabolomic study performed in the cardiac tissue of the animals showed that the treatment with vericiguat was able to partially restore the decrease of cardiac 6-phosphogluconate and D-ribose 5-phosphate (a main intermediate of the oxidative phase and one of the final products of the non-oxidative phase, respectively, of the PPP) observed in the obese control group. In concordance with the metabolomics results, the cardiac phosphoproteomic analysis revealed that vericiguat increased the levels of phosphorylated 6-phosphogluconolactonase and 6-phosphogluconate dehydrogenase, two pivotal enzymes of the oxidative phase of the PPP whose phosphorylation have been related with an enhancement of its activity [117]. The PPP is a key metabolic route for cardiac cells, and its modulation is considered a promising strategy to manage several cardiometabolic pathologies [118]. Cardiac metabolic reprogramming by stimulation of the PPP prevents cardiac dysfunction and attenuates oxidative stress in the myocardium [119–121]. In fact, endomyocardial biopsies from HFpEF patients have reduced PPP metabolites compared to non-disease controls [122]. The steady state levels of antioxidant molecules (also at cardiac level) are largely dependent on the generation of NADPH (reduced nicotinamide adenine dinucleotide phosphate), which is used to maintain glutathione and thioredoxin in the reduced state [123]. Since the PPP is one of the main metabolic pathways that controls the biosynthesis of NADPH [124], this molecule might constitute the link between the upregulation of PPP and the antioxidant response induced by the treatment with vericiguat in our animal model.

Lastly, the treatment with vericiguat attenuated the decline of the levels of cardiac arginine detected in the obese control group. It is known that an increase in the myocardial arginine levels is linked to an improvement in cardiac function [125]. The attenuation of the arginine decline by vericiguat could contribute to the beneficial effects in the obese ZSF1 rat HFpEF model.

5. Conclusions

The prevalence of HFpEF is increasing, while treatment options are insufficient. Early metabolic changes, bioenergetic perturbations, and cardiac structural remodelling are pivotal in the pathogenic HFpEF cascade, providing targets that may aid in the development of more precise therapies. We demonstrate that the treatment with an sGC stimulator (vericiguat) elicits beneficial functional and metabolic responses at the cardiac level in an animal model of HFpEF when administered at an early-stage of the disease (Fig. 9). Vericiguat induced a reduction of hypertrophy and fibrosis, and a significant improvement of diastolic dysfunction. The treatment with vericiguat improved mitochondrial function, increased the levels of pivotal mitochondrial proteins involved in antioxidant processes, and stimulated cardioprotective metabolic processes such as the pentose phosphate pathway. Our results could contribute to a better understanding of the potential effects of sGC stimulation on the pathophysiological mechanisms that participate in the development and progression of HFpEF. Those findings also underscore cardiac metabolism and mitochondrial function as novel therapeutic targets of sGC stimulators in early-stage HFpEF.

6. Limitations

The available animal models of HFpEF do not fully reproduce the human disease and mimic only parts of the clinical phenotypes. Therefore, the relevance of these findings needs to be confirmed in the human setting. Both the female and the male obese ZSF1 rats are relevant animal models for HFpEF with multiple comorbidities, with some metabolic differences between them, and both of them suitable for investigating novel therapeutic interventions; so, the effects of vericiguat reported in this work should be studied in the future in female rats with HFpEF. The mechanisms that mediate the favourable effects elicited by vericiguat in early-stage HFpEF need to be further explored

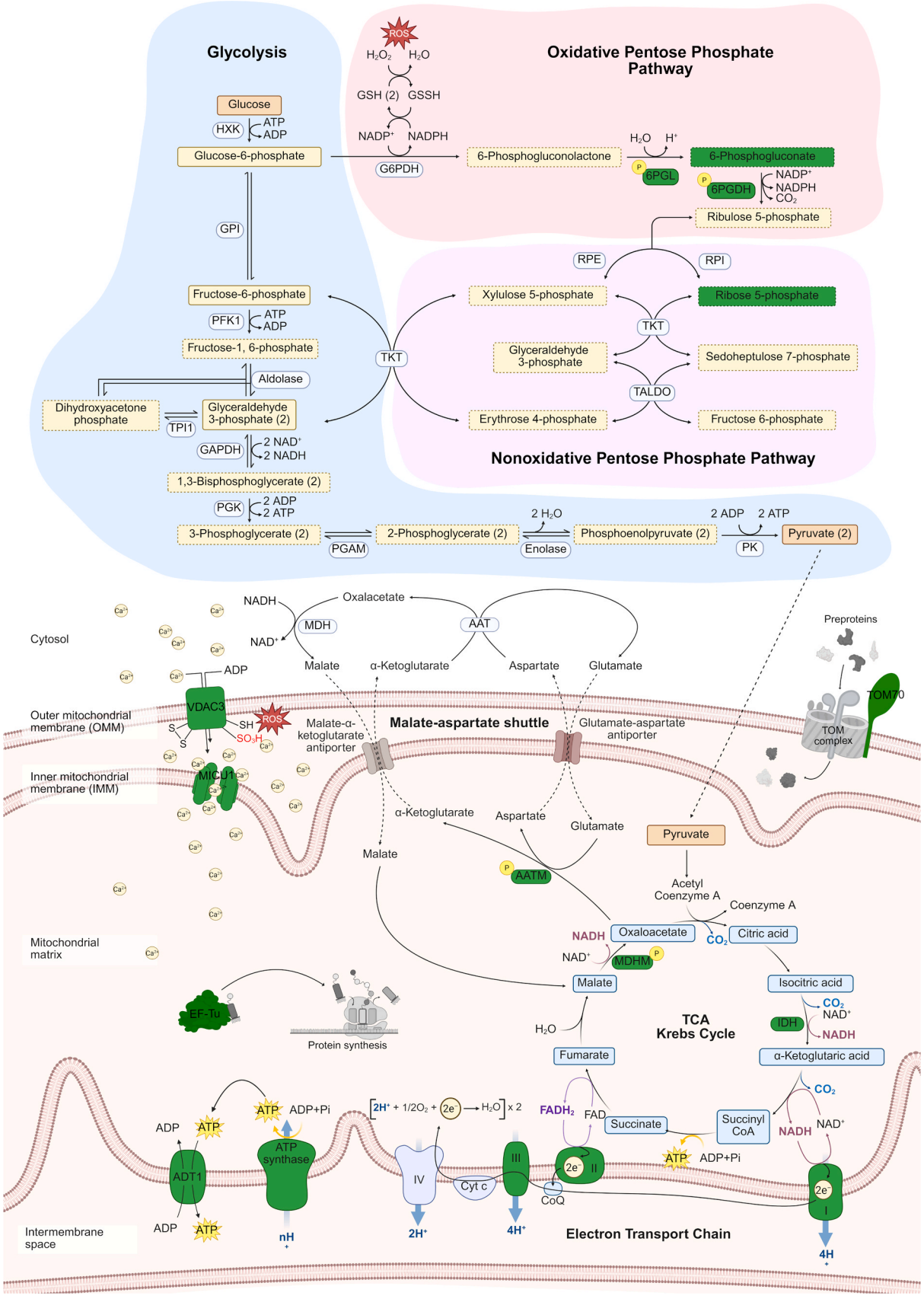

(caption on next page)

Fig. 9. Potential metabolic pathways modulated and/or preserved by that the soluble guanylate cyclase stimulator vericiguat. Illustrative representation of the pentose phosphate pathway (PPP), the malate-aspartate shuttle, the Krebs cycle and the electron transport chain, highlighting (in green) metabolites and enzymes whose levels could be modulated or prevented following vericiguat treatment. Created in https://BioRender.com. The solid arrows denote the key steps within the metabolic pathways, while the dashed arrows signify the involvement of additional steps. AAT: aspartate aminotransferase, AATM: aspartate aminotransferase (mitochondrial), ADP: adenosine diphosphate, ADT1: ADP/ATP translocase 1, ATP: adenosine triphosphate, CoQ: coenzyme Q, Cyt C: cytochrome C, EF-Tu: elongation factor Tu (mitochondrial), FAD: flavin adenine dinucleotide, FADH2: flavin adenine dinucleotide (reduced form), GAPDH: glyceraldehyde-3-phosphate dehydrogenase, G6PDH: glucose-6-phosphate dehydrogenase, GPI: glucose-6-phosphate isomerase, GSH: glutathione (reduced form), GSSH: glutathione disulfide (oxidized form), HXK: hexokinase, I: NADH dehydrogenase, IDH: Isocitrate dehydrogenase, II: Succinate dehydrogenase, III: Cytochrome bc1 complex, IV: cytochrome c oxidase, MDH: malate dehydrogenase, MDHM: malate dehydrogenase (mitochondrial), MICU1: mitochondrial calcium uptake protein 1, NAD+ : nicotinamide adenine dinucleotide (oxidized form), NADH: nicotinamide adenine dinucleotide (reduced form), NADP+ : nicotinamide adenine dinucleotide phosphate (oxidized form), NADPH: nicotinamide adenine dinucleotide phosphate (reduced form), PGAM: phosphoglycerate mutase, PGK: phosphoglycerate kinase, PFK1: phosphofructokinase 1, PK: pyruvate kinase, RPE: ribulose-5-phosphate epimerase, RP1: ribulose-5-phosphate isomerase 1, TKT: transketolase, TALDO: Transaldolase, TPI1: triosephosphate isomerase 1, TOM70: mitochondrial import receptor subunit TOM70, VDAC3: non-selective voltage-gated ion channel VDAC3 (Voltage-Dependent Anion-Selective Channel Protein 3), 6PGL: 6-phosphogluconolactonase, 6PGDH: 6-phosphogluconate dehydrogenase.

and extended. We have experienced significant obstacles in the quantification of mitochondrial area, as well as shape descriptors such as perimeter, roundness, circularity, Feret's diameter and aspect ratio in LV samples from obese animals. These samples presented highly disorganized fibres in which mitochondria were fragmented and/or swollen, and it was not possible to properly identify and trace them for an individual and accurate quantification. This limitation implies a small number of quantified mitochondria in the obese control group.

CRediT authorship contribution statement

Inês N. Alves: Supervision, Resources, Methodology, Investigation, Formal analysis. **Sandra Moraña-Fernández:** Writing – review & editing, Writing – original draft, Visualization, Supervision, Software, Methodology, Investigation, Formal analysis, Data curation. **Cláudia Sousa-Mendes:** Supervision, Resources, Methodology, Investigation. **Alana Aragón-Herrera:** Writing – review & editing, Writing – original draft, Visualization, Validation, Supervision, Resources, Methodology, Investigation, Formal analysis. **Carlos Tilves-Bellas:** Data curation, Formal analysis. **Francisca Lago:** Writing – review & editing, Writing – original draft, Visualization, Validation, Supervision, Resources, Project administration, Methodology, Formal analysis, Conceptualization. **Alexandre Gonçalves:** Supervision, Resources, Methodology, Investigation. **Juliana Pereira Morais:** Supervision, Resources, Methodology, Investigation, Formal analysis. **Xocas Vázquez-Abuín:** Writing – review & editing, Writing – original draft, Visualization, Supervision, Software, Methodology, Investigation, Formal analysis, Data curation. **Esther Roselló-Lletí:** Resources. **Javier García-Seara:** Resources, Formal analysis. **Manuel Portolés:** Resources. **Susana B. Bravo:** Validation, Software, Resources, Methodology, Formal analysis. **Inês Falcão-Pires:** Supervision, Methodology, Investigation, Formal analysis. **Peter Sandner:** Writing – review & editing, Supervision, Resources, Project administration. **Estefanía Tarazón:** Resources. **Karen Thomitzek:** Supervision, Resources, Project administration. **Manuel Otero-Santiago:** Resources, Formal analysis. **Pablo de la Fuente-López:** Writing – review & editing, Data curation. **José Ramón González-Juanatey:** Validation, Supervision, Resources. **Sandra Feijóo-Bandín:** Writing – review & editing, Writing – original draft, Visualization, Validation, Supervision, Resources, Project administration, Methodology, Formal analysis, Conceptualization. **Alexandre Rodrigues:** Supervision, Resources, Methodology, Investigation. **Oreste Gualillo:** Validation, Resources.

Funding sources

This work was supported by a research grant of Bayer AG (DEU), the National Institute of Health "Fondo de Investigaciones Sanitarias del Instituto de Salud Carlos III" Madrid, Spain [PI21/01145, PI24/00114 and CIBER de Enfermedades Cardiovasculares (CIBERCV)]; Axencia Galega de Innovación (GAIN): Axudas do programa de consolidación e estruturación de unidades de investigación competitivas (GPC IN607B 2021 108 and GPC IN607B 2024–02). S.M.-F. was funded by a predoctoral research grant from GAIN-Xunta de Galicia (Spain), X.V.-A. was funded by Sociedad Española de Cardiología (RLD_SEC2016 and SECAINC-INV-ICC 23/02) and A.A.-H. postdoctoral contract is funded by the Sara Borrell Program of the Instituto de Salud Carlos III (ISCIII) and previously was funded by a postdoctoral research grant from Health Research Institute of Santiago de Compostela (IDIS) and Foundation of IDIS (FIDIS).

Declaration of Competing Interest

The authors declare the following financial interests/personal relationships which may be considered as potential competing interests: Peter Sandner and Karen Thomitzek reports a relationship with Bayer AG, Pharmaceuticals that includes: employment. If there are other authors, they declare that they have no known competing financial interests or personal relationships that could have appeared to influence the work reported in this paper.

Acknowledgements

We would like to express our gratitude to Professor Daniele Bani and Daniele Guasti (Department of Experimental & Clinical Medicine, Section of Anatomy & Histology, University of Florence, Italy) for their guidance in understanding and analysing mitochondrial micrographs from electron transmission microscopy.

Appendix A. Supporting information

Supplementary data associated with this article can be found in the online version at doi:10.1016/j.biopha.2025.118439.

Data Availability

Data will be made available on request.

References

[1] M. Carlström, E. Weitzberg, J.O. Lundberg, Nitric oxide signaling and regulation in the cardiovascular system: recent advances, Pharm. Rev. 76 (2024) 1038–1062, https://doi.org/10.1124/pharmrev.124.001060.
[2] Q. Fu, Y. Wang, C. Yan, Y.K. Xiang, Phosphodiesterase in heart and vessels: from physiology to diseases, Physiol. Rev. 104 (2024) 765–834, https://doi.org/10.1152/physrev.00015.2023.
[3] M. Emdin, A. Aimo, V. Castiglione, G. Vergaro, G. Georgiopoulos, L.F. Saccaro, C. M. Lombardi, C. Passino, E. Cerbai, M. Metra, M. Senni, Targeting cyclic guanosine monophosphate to treat heart failure, J. Am. Coll. Cardiol. 76 (2020) 1795–1807, https://doi.org/10.1016/j.jacc.2020.08.031.
[4] M. Park, P. Sandner, T. Krieg, cGMP at the centre of attention: emerging strategies for activating the cardioprotective PKG pathway, Basic Res Cardiol. 113 (2018) 24, https://doi.org/10.1007/s00395-018-0679-9.
[5] J. Xia, N. Hui, L. Tian, C. Liang, J. Zhang, J. Liu, J. Wang, X. Ren, X. Xie, K. Wang, Development of vericiguat: the first soluble guanylate cyclase (sGC) stimulator launched for heart failure with reduced ejection fraction (HFrEF), Biomed.

Pharmacother. 149 (2022) 112894, https://doi.org/10.1016/j.biopha.2022.112894.
[6] P. Sandner, A. Vakalopoulos, M.G. Hahn, J.-P. Stasch, M. Follmann, Soluble guanylate cyclase stimulators and their potential use: a patent review, Expert Opin. Ther. Pat. 31 (2021) 203–222, https://doi.org/10.1080/13543776.2021.1866538.
[7] M. Follmann, J. Ackerstaff, G. Redlich, F. Wunder, D. Lang, A. Kern, P. Fey, N. Griebenow, W. Kroh, E.-M. Becker-Pelster, A. Kretschmer, V. Geiss, V. Li, A. Straub, J. Mittendorf, R. Jautelat, H. Schirok, K.-H. Schlemmer, K. Lustig, M. Gerisch, A. Knorr, H. Tinel, T. Mondritzki, H. Trübel, P. Sandner, J.-P. Stasch, Discovery of the soluble guanylate cyclase stimulator vericiguat (BAY 1021189) for the treatment of chronic heart failure, J. Med Chem. 60 (2017) 5146–5161, https://doi.org/10.1021/acs.jmedchem.7b00449.
[8] K. Boden, P. Sandner, L. Roessig, J. Vogel, J.A. Chirinos, T. Mondritzki, Vericiguat improves aortic wave reflection parameters in a new preclinical model of hypertension, Circ. Heart Fail 15 (2022), https://doi.org/10.1161/CIRCHEARTFAILURE.121.008735.
[9] S. Breitenstein, L. Roessig, P. Sandner, K.S. Lewis, Novel sGC Stimulators and sGC Activators for the Treatment of Heart Failure, in: 2016: pp. 225–247. https://doi.org/10.1007/164_2016_100.
[10] R.J. Mentz, A. Stebbins, J. Butler, C.-E. Chiang, J.A. Ezekowitz, A.F. Hernandez, R. Hilkert, C.S.P. Lam, K. McDonald, C.M. O'Connor, B. Pieske, P. Ponikowski, L. Roessig, N.K. Sweitzer, A.A. Voors, K.J. Anstrom, P.W. Armstrong, Recurrent hospitalizations and response to vericiguat in heart failure and reduced ejection fraction, JACC Heart Fail 12 (2024) 839–846, https://doi.org/10.1016/j.jchf.2023.12.005.
[11] J. Butler, Y. Zheng, M.S. Khan, D. Bonderman, L.H. Lund, C.R. deFilippi, R. O. Blaustein, J.A. Ezekowitz, C. Freitas, A.F. Hernandez, C.M. O'Connor, A. A. Voors, C.M. Westerhout, C.S.P. Lam, P.W. Armstrong, Ejection fraction, biomarkers, and outcomes and impact of vericiguat on outcomes across EF in Victoria, JACC Heart Fail 11 (2023) 583–592, https://doi.org/10.1016/j.jchf.2022.12.014.
[12] C.S.P. Lam, I.L. Piña, Y. Zheng, D. Bonderman, A.-C. Pouleur, C. Saldarriaga, B. Pieske, R.O. Blaustein, R. Nkulikiyinka, C.M. Westerhout, P.W. Armstrong, Age, sex, and outcomes in heart failure with reduced EF, JACC Heart Fail 11 (2023) 1246–1257, https://doi.org/10.1016/j.jchf.2023.06.020.
[13] P.W. Armstrong, C.S.P. Lam, K.J. Anstrom, J. Ezekowitz, A.F. Hernandez, C. M. O'Connor, B. Pieske, P. Ponikowski, S.J. Shah, S.D. Solomon, A.A. Voors, L. She, V. Vlajnic, F. Carvalho, L. Bamber, R.O. Blaustein, L. Roessig, J. Butler, Effect of vericiguat vs placebo on quality of life in patients with heart failure and preserved ejection fraction, JAMA 324 (2020) 1512, https://doi.org/10.1001/jama.2020.15922.
[14] B. Pieske, A.P. Maggioni, C.S.P. Lam, E. Pieske-Kraigher, G. Filippatos, J. Butler, P. Ponikowski, S.J. Shah, S.D. Solomon, A.-V. Scalise, K. Mueller, L. Roessig, M. Gheorghiade, Vericiguat in patients with worsening chronic heart failure and preserved ejection fraction: results of the SOluble guanylate cyclase stimulator in heArT failure patients with PRESERVED EF (SOCRATES-PRESERVED) study, Eur. Heart J. 38 (2017) 1119–1127, https://doi.org/10.1093/eurheartj/ehw593.
[15] D. Kolijn, S. Pabel, Y. Tian, M. Lódi, M. Herwig, A. Carrizzo, S. Zhazykbayeva, Á. Kovács, G.Á. Fülöp, I. Falcão-Pires, P.H. Reusch, S. Van Linthout, Z. Papp, L. van Heerebeek, C. Vecchione, L.S. Maier, M. Ciccarelli, C. Tschöpe, A. Mügge, Z. Bagi, S. Sossalla, N. Hamdani, Empagliflozin improves endothelial and cardiomyocyte function in human heart failure with preserved ejection fraction via reduced pro-inflammatory-oxidative pathways and protein kinase Gα oxidation, Cardiovasc Res 117 (2021) 495–507, https://doi.org/10.1093/cvr/cvaa123.
[16] C.R. deFilippi, P. Shah, S.J. Shah, W. Alemayehu, C.S.P. Lam, J. Butler, L. Roessig, C.M. O'Connor, C.M. Westerhout, P.W. Armstrong, Proteomics identify clinical phenotypes and predict functional outcomes in heart failure with preserved ejection fraction: insights from VITALITY-HFpEF, Circ. Heart Fail 17 (2024), https://doi.org/10.1161/CIRCHEARTFAILURE.124.011792.
[17] M.A. Konstam, Exploring ejection fraction range in heart failure clinical trials, JACC Heart Fail 11 (2023) 593–595, https://doi.org/10.1016/j.jchf.2023.01.017.
[18] R. Mollace, F. Scarano, I. Bava, C. Carresi, J. Maiuolo, A. Tavernese, M. Gliozzi, V. Musolino, S. Muscoli, E. Palma, C. Muscoli, D. Salvemini, M. Federici, R. Macrì, V. Mollace, Modulation of the nitric oxide/cGMP pathway in cardiac contraction and relaxation: potential role in heart failure treatment, Pharm. Res 196 (2023) 106931, https://doi.org/10.1016/j.phrs.2023.106931.
[19] J.E. Udelson, G.D. Lewis, S.J. Shah, M.R. Zile, M.M. Redfield, J. Burnett, J. Parker, J.P. Seferovic, P. Wilson, R.S. Mittleman, A.T. Profy, M.A. Konstam, Effect of praliciguat on peak rate of oxygen consumption in patients with heart failure with preserved ejection fraction, JAMA 324 (2020) 1522, https://doi.org/10.1001/jama.2020.16641.
[20] J. Mira Hernandez, E.Y. Shen, C.Y. Ko, Z. Hourani, E.R. Spencer, D. Smoliarchuk, J. Bossuyt, H. Granzier, D.M. Bers, B. Hegyi, Differential sex-dependent susceptibility to diastolic dysfunction and arrhythmia in cardiomyocytes from obese diabetic heart failure with preserved ejection fraction model, Cardiovasc Res. (2024), https://doi.org/10.1093/cvr/cvae070.
[21] Q. Sun, B. Güven, C.S. Wagg, A. Almeida de Oliveira, H. Silver, L. Zhang, B. Chen, K. Wei, E.B. Ketema, Q.G. Karwi, K.L. Persad, J. Vu, F. Wang, J.R.B. Dyck, G. Y. Oudit, G.D. Lopaschuk, Mitochondrial fatty acid oxidation is the major source of cardiac adenosine triphosphate production in heart failure with preserved ejection fraction, Cardiovasc Res. 120 (2024) 360–371, https://doi.org/10.1093/cvr/cvae006.
[22] A. Lozhkin, A.E. Vendrov, R. Ramos-Mondragón, C. Canugovi, M.D. Stevenson, T. J. Herron, S.L. Hummel, C.A. Figueroa, D.E. Bowles, L.L. Isom, M.S. Runge, N. R. Madamanchi, Mitochondrial oxidative stress contributes to diastolic dysfunction through impaired mitochondrial dynamics, Redox Biol. 57 (2022) 102474, https://doi.org/10.1016/j.redox.2022.102474.
[23] Guide for the Care and Use of Laboratory Animals, National Academies Press, Washington, D.C., 2011. https://doi.org/10.17226/12910.
[24] A. Schauer, V. Adams, A. Augstein, A. Jannasch, R. Draskowski, V. Kirchhoff, K. Goto, J. Mittag, R. Galli, A. Männel, P. Barthel, A. Linke, E.B. Winzer, Sacubitril/Valsartan improves diastolic function but not skeletal muscle function in a rat model of HFpEF, Int J. Mol. Sci. 22 (2021) 3570, https://doi.org/10.3390/ijms22073570.
[25] W.B. van Ham, E.L. Kessler, M.I.F.J. Oerlemans, M.L. Handoko, J.P.G. Sluijter, T. A.B. van Veen, H.M. den Ruijter, S.C.A. de Jager, Clinical phenotypes of heart failure with preserved ejection fraction to select preclinical animal models, JACC Basic Transl. Sci. 7 (2022) 844–857, https://doi.org/10.1016/j.jacbts.2021.12.009.
[26] Q.A.J. Hagdorn, G.P.L. Bossers, A.-M.C. Koop, A. Piek, T.R. Eijgenraam, D.E. van der Feen, H.H.W. Silljé, R.A. de Boer, R.M.F. Berger, A novel method optimizing the normalization of cardiac parameters in small animal models: the importance of dimensional indexing, Am. J. Physiol. Heart Circ. Physiol. 316 (2019) H1552–H1557, https://doi.org/10.1152/ajpheart.00182.2019.
[27] Ilka Mathar, Mira Pavkovic, Nina Scheerer, Elke Hartmann, Peter Sandner, Abstract 15553: the sGC stimulator vericiguat improved outcome in a rodent model of heart failure with preserved ejection fraction (HFpEF), Circulation 138 (2018).
[28] D. Miranda-Silva, P. G. Rodrigues, E. Alves, D. Rizo, A.C.R.G. Fonseca, T. Lima, F. Baganha, G. Conceição, C. Sousa, A. Gonçalves, I. Miranda, F. Vasques-Nóvoa, J. Magalhães, A. Leite-Moreira, I. Falcão-Pires, Mitochondrial reversible changes determine diastolic function adaptations during myocardial (Reverse) remodeling, Circ. Heart Fail 13 (2020), https://doi.org/10.1161/CIRCHEARTFAILURE.119.006170.
[29] X. Aiyasiding, H.-H. Liao, H. Feng, N. Zhang, Z. Lin, W. Ding, H. Yan, Z.-Y. Zhou, Q.-Z. Tang, Liquiritin attenuates pathological cardiac hypertrophy by activating the PKA/LKB1/AMPK pathway, Front. Pharm. 13 (2022), https://doi.org/10.3389/fphar.2022.870699.
[30] P.G. Rodrigues, D. Miranda-Silva, S.M. Costa, C. Barros, N. Hamdani, C. Moura, M.J. Mendes, C. Sousa-Mendes, F. Trindade, D. Fontoura, R. Vitorino, W.A. Linke, A.F. Leite-Moreira, I. Falcão-Pires, Early myocardial changes induced by doxorubicin in the nonfailing dilated ventricle, Am. J. Physiol. Heart Circ. Physiol. 316 (2019) H459–H475, https://doi.org/10.1152/ajpheart.00401.2018.
[31] C. Mas-Bargues, E. García-Domínguez, C. Borrás, Recent approaches to determine static and dynamic redox State-Related parameters, Antioxidants 11 (2022) 864, https://doi.org/10.3390/antiox11050864.
[32] C. Doerrier, L.F. Garcia-Souza, G. Krumschnabel, Y. Wohlfarter, A.T. Mészáros, E. Gnaiger, High-Resolution FluoRespirometry and OXPHOS Protocols for Human Cells, Permeabilized Fibers from Small Biopsies of Muscle, and Isolated Mitochondria, in: 2018: pp. 31–70. https://doi.org/10.1007/978-1-4939-7831-1_3.
[33] A. Aragón-Herrera, S. Feijóo-Bandín, X. Vázquez-Abuín, L. Anido-Varela, S. Moraña-Fernández, S.B. Bravo, E. Tarazón, E. Roselló-Lletí, M. Portolés, J. García-Seara, J. Seijas, D. Rodríguez-Penas, D. Bani, O. Gualillo, J.R. González-Juanatey, F. Lago, Human recombinant relaxin-2 (serelaxin) regulates the proteome, lipidome, lipid metabolism and inflammatory profile of rat visceral adipose tissue, Biochem. Pharm. 223 (2024) 116157, https://doi.org/10.1016/j.bcp.2024.116157.
[34] S. Moraña-Fernández, X. Vázquez-Abuín, A. Aragón-Herrera, L. Anido-Varela, J. García-Seara, Ó. Otero-García, D. Rodríguez-Penas, M. Campos-Toimil, M. Otero-Santiago, A. Rodrigues, A. Gonçalves, J. Pereira Morais, I.N. Alves, C. Sousa-Mendes, I. Falcão-Pires, J.R. González-Juanatey, S. Feijóo-Bandín, F. Lago, Cardiometabolic effects of sacubitril/valsartan in a rat model of heart failure with preserved ejection fraction, Biochem. Pharm. 230 (2024) 116571, https://doi.org/10.1016/j.bcp.2024.116571.
[35] Y. Perez-Riverol, C. Bandla, D.J. Kundu, S. Kamatchinathan, J. Bai, S. Hewapathirana, N.S. John, A. Prakash, M. Walzer, S. Wang, J.A. Vizcaíno, The PRIDE database at 20 years: 2025 update, Nucleic Acids Res. 53 (2025) D543–D553, https://doi.org/10.1093/nar/gkae1011.
[36] J. Barr, J. Caballería, I. Martínez-Arranz, A. Domínguez-Díez, C. Alonso, J. Muntané, M. Pérez-Cormenzana, C. García-Monzón, R. Mayo, A. Martín-Duce, M. Romero-Gómez, O.Lo Iacono, J. Tordjman, R.J. Andrade, M. Pérez-Carreras, Y. Le Marchand-Brustel, A. Tran, C. Fernández-Escalante, E. Arévalo, M. García-Unzueta, K. Clement, J. Crespo, P. Gual, M. Gómez-Fleitas, M.L. Martínez-Chantar, A. Castro, S.C. Lu, M. Vázquez-Chantada, J.M. Mato, Obesity-Dependent metabolic signatures associated with nonalcoholic fatty liver disease progression, J. Proteome Res. 11 (2012) 2521–2532, https://doi.org/10.1021/pr201223p.
[37] A. Aragón-Herrera, S. Feijóo-Bandín, S. Moraña-Fernández, L. Anido-Varela, E. Roselló-Lletí, M. Portolés, E. Tarazón, R. Lage, I. Moscoso, L. Barral, D. Bani, M. Bigazzi, O. Gualillo, J.R. González-Juanatey, F. Lago, Relaxin has beneficial effects on liver lipidome and metabolic enzymes, FASEB J. 35 (2021), https://doi.org/10.1096/fj.202002620RR.
[38] I. Martínez-Arranz, R. Mayo, M. Pérez-Cormenzana, I. Mincholé, L. Salazar, C. Alonso, J.M. Mato, Enhancing metabolomics research through data mining, J. Proteom. 127 (2015) 275–288, https://doi.org/10.1016/j.jprot.2015.01.019.
[39] Y.N.V. Reddy, A.K. Asokan, R.P. Frantz, A. Hemnes, P.M. Hassoun, J. Barnard, E. Horn, J.A. Leopold, F. Rischard, E.B. Rosenzweig, N.S. Hill, S.C. Erzurum, G. J. Beck, J.E. Finet, G. Grunig, C.L. Jellis, S.C. Mathai, C.E. Simpson, W.H.W. Tang,

K.S. Nair, B.A. Borlaug, PVDOMICS study group, metabolomic evidence of biological overlap with HFpEF in a subset of pulmonary arterial hypertension, Am. J. Respir. Crit. Care Med. (2025).
[40] S. Chen, Y. Zou, C. Song, K. Cao, K. Cai, Y. Wu, Z. Zhang, D. Geng, W. Sun, N. Ouyang, N. Zhang, Z. Li, G. Sun, Y. Zhang, Y. Sun, Y. Zhang, The role of glycolytic metabolic pathways in cardiovascular disease and potential therapeutic approaches, Basic Res. Cardiol. 118 (2023) 48, https://doi.org/10.1007/s00395-023-01018-w.
[41] T. Petit, G. Claessen, M. Claeys, A. La Gerche, P. Claus, S. Ghysels, M. Delcroix, A. Ciarka, W. Droogne, J. Van Cleemput, R. Willems, J. Voigt, J. Bogaert, S. Janssens, Right ventricular and cyclic guanosine monophosphate signalling abnormalities in stages b and c of heart failure with preserved ejection fraction, ESC Heart Fail 8 (2021) 4661–4673, https://doi.org/10.1002/ehf2.13514.
[42] B.A. Borlaug, K. Sharma, S.J. Shah, J.E. Ho, Heart failure with preserved ejection fraction, J. Am. Coll. Cardiol. 81 (2023) 1810–1834, https://doi.org/10.1016/j.jacc.2023.01.049.
[43] C.E. Hamo, C. DeJong, N. Hartshorne-Evans, L.H. Lund, S.J. Shah, S. Solomon, C. S.P. Lam, Heart failure with preserved ejection fraction, Nat. Rev. Dis. Prim. 10 (2024) 55, https://doi.org/10.1038/s41572-024-00540-y.
[44] P. Campbell, F.H. Rutten, M.M. Lee, N.M. Hawkins, M.C. Petrie, Heart failure with preserved ejection fraction: everything the clinician needs to know, Lancet 403 (2024) 1083–1092, https://doi.org/10.1016/S0140-6736(23)02756-3.
[45] Y. Saito, M. Obokata, T. Harada, K. Kagami, N. Wada, Y. Okumura, H. Ishii, Prognostic benefit of early diagnosis with exercise stress testing in heart failure with preserved ejection fraction, Eur. J. Prev. Cardiol. 30 (2023) 902–911, https://doi.org/10.1093/eurjpc/zwad127.
[46] M.A. Pfeffer, A.M. Shah, B.A. Borlaug, Heart failure with preserved ejection fraction in perspective, Circ. Res. 124 (2019) 1598–1617, https://doi.org/10.1161/CIRCRESAHA.119.313572.
[47] Z. Cai, C. Wu, Y. Xu, J. Cai, M. Zhao, L. Zu, The NO-cGMP-PKG axis in HFpEF: from pathological mechanisms to potential therapies, Aging Dis. 14 (2023) 46–62, https://doi.org/10.14336/AD.2022.0523.
[48] F. Capone, C. Sotomayor-Flores, D. Bode, R. Wang, D. Rodolico, S. Strocchi, G. G. Schiattarella, Cardiac metabolism in HFpEF: from fuel to signalling, Cardiovasc Res. 118 (2023) 3556–3575, https://doi.org/10.1093/cvr/cvac166.
[49] B. Ye, A.D. Bradshaw, J.E. Abrahante, J.A. Dragon, T.N. Häußler, S.P. Bell, F. Hirashima, M. LeWinter, M.R. Zile, M. Meyer, Left ventricular gene expression in heart failure with preserved ejection Fraction—Profibrotic and proinflammatory pathways and genes, Circ. Heart Fail 16 (2023), https://doi.org/10.1161/CIRCHEARTFAILURE.123.010395.
[50] A.U. Fayyaz, M. Eltony, L.J. Prokop, K.E. Koepp, B.A. Borlaug, S. Dasari, M. C. Bois, K.B. Margulies, J.J. Maleszewski, Y. Wang, M.M. Redfield, Pathophysiological insights into HFpEF from studies of human cardiac tissue, Nat. Rev. Cardiol. (2024), https://doi.org/10.1038/s41569-024-01067-1.
[51] P. Sandner, M. Follmann, E. Becker-Pelster, M.G. Hahn, C. Meier, C. Freitas, L. Roessig, J. Stasch, Soluble GC stimulators and activators: past, present and future, Br. J. Pharm. 181 (2024) 4130–4151, https://doi.org/10.1111/bph.15698.
[52] R. Mollace, F. Scarano, I. Bava, C. Carresi, J. Maiuolo, A. Tavernese, M. Gliozzi, V. Musolino, S. Muscoli, E. Palma, C. Muscoli, D. Salvemini, M. Federici, R. Macrì, V. Mollace, Modulation of the nitric oxide/cGMP pathway in cardiac contraction and relaxation: potential role in heart failure treatment, Pharm. Res 196 (2023) 106931, https://doi.org/10.1016/j.phrs.2023.106931.
[53] D. Miranda-Silva, R.C.I. Wüst, G. Conceição, P. Gonçalves-Rodrigues, N. Gonçalves, A. Gonçalves, D.W.D. Kuster, A.F. Leite-Moreira, J. van der Velden, J.M. de Sousa Beleza, J. Magalhães, G.J.M. Stienen, I. Falcão-Pires, Disturbed cardiac mitochondrial and cytosolic calcium handling in a metabolic risk-related rat model of heart failure with preserved ejection fraction, Acta Physiol. 228 (2020), https://doi.org/10.1111/apha.13378.
[54] A. Schauer, R. Draskowski, A. Jannasch, V. Kirchhoff, K. Goto, A. Männel, P. Barthel, A. Augstein, E. Winzer, M. Tugtekin, S. Labeit, A. Linke, V. Adams, ZSF1 rat as animal model for HFpEF: development of reduced diastolic function and skeletal muscle dysfunction, ESC Heart Fail 7 (2020) 2123–2134, https://doi.org/10.1002/ehf2.12915.
[55] A. Schauer, V. Adams, S. Kämmerer, E. Langner, A. Augstein, P. Barthel, A. Männel, G. Fabig, P.K.N. Alves, M. Günscht, A. El-Armouche, T. Müller-Reichert, A. Linke, E.B. Winzer, Empagliflozin improves diastolic function in HFpEF by restabilizing the mitochondrial respiratory chain, Circ. Heart Fail 17 (2024), https://doi.org/10.1161/CIRCHEARTFAILURE.123.011107.
[56] S.J. Simmonds, M.O.J. Grootaert, I. Cuijpers, P. Carai, N. Geuens, M. Herwig, P. Baatsen, N. Hamdani, A. Luttun, S. Heymans, E.A.V. Jones, Pericyte loss initiates microvascular dysfunction in the development of diastolic dysfunction, Eur. Heart J. Open 4 (2023), https://doi.org/10.1093/ehjopen/oead129.
[57] S.J. Guivala, K.A. Bode, J.G. Okun, E. Kartal, E. Schwedhelm, L.V. Pohl, S. Werner, S. Erbs, H. Thiele, P. Büttner, Interactions between the gut microbiome, associated metabolites and the manifestation and progression of heart failure with preserved ejection fraction in ZSF1 rats, Cardiovasc Diabetol. 23 (2024) 299, https://doi.org/10.1186/s12933-024-02398-6.
[58] G. Liu, C.M. Shea, J.E. Jones, G.M. Price, W. Warren, E. Lonie, S. Yan, M. G. Currie, A.T. Profy, J.L. Masferrer, D.P. Zimmer, Praliciguat inhibits progression of diabetic nephropathy in ZSF1 rats and suppresses inflammation and apoptosis in human renal proximal tubular cells, Am. J. Physiol. Ren. Physiol. 319 (2020) F697–F711, https://doi.org/10.1152/ajprenal.00003.2020.
[59] V. Reverte, F. Rodriguez, L. Oltra, J.M. Moreno, M.T. Llinás, C.M. Shea, C. D. Schwartzkopf, E.S. Buys, J.L. Masferrer, F.J. Salazar, SGLT2 inhibition potentiates the cardiovascular, renal, and metabolic effects of sGC stimulation in hypertensive rats with prolonged exposure to high-fat diet, Am. J. Physiol. Heart Circ. Physiol. 322 (2022) H523–H536, https://doi.org/10.1152/ajpheart.00386.2021.
[60] R. Patel, Y. Fu, S. Khang, A.M. Benardeau, S.C. Thomson, V. Vallon, Responses in blood pressure and kidney function to soluble guanylyl cyclase stimulation or activation in normal and diabetic rats, Nephron 147 (2023) 281–300, https://doi.org/10.1159/000526934.
[61] J.P. Hanrahan, J.P. Seferovic, J.D. Wakefield, P.J. Wilson, J.G. Chickering, J. Jung, K.E. Carlson, D.P. Zimmer, A.L. Frelinger, A.D. Michelson, L. Morrow, M. Hall, M.G. Currie, G.T. Milne, A.T. Profy, An exploratory, randomised, placebo-controlled, 14 day trial of the soluble guanylate cyclase stimulator praliciguat in participants with type 2 diabetes and hypertension, Diabetologia 63 (2020) 733–743, https://doi.org/10.1007/s00125-019-05062-x.
[62] L.S. Hoffmann, J. Etzrodt, L. Willkomm, A. Sanyal, L. Scheja, A.W.C. Fischer, J.-P. Stasch, W. Bloch, A. Friebe, J. Heeren, A. Pfeifer, Stimulation of soluble guanylyl cyclase protects against obesity by recruiting brown adipose tissue, Nat. Commun. 6 (2015) 7235, https://doi.org/10.1038/ncomms8235.
[63] P. Jungtanasomboon, S. Nussaro, H. Winwan, P. Suebthawinkul, P. Boonpala, V. N.K. Dong, N. Saengklub, S. Kumphune, Y. Panyasing, A. Kijtawornrat, Vericiguat preserved cardiac function and mitochondrial quality in a rat model of mitral regurgitation, Life Sci. 328 (2023) 121929, https://doi.org/10.1016/j.lfs.2023.121929.
[64] X. Zeng, H. Zhang, T. Xu, X. Mei, X. Wang, Q. Yang, Z. Luo, Q. Zeng, D. Xu, H. Ren, Vericiguat attenuates doxorubicin-induced cardiotoxicity through the PRKG1/PINK1/STING axis, Transl. Res. 273 (2024) 90–103, https://doi.org/10.1016/j.trsl.2024.07.005.
[65] P.W. Armstrong, L. Roessig, M.J. Patel, K.J. Anstrom, J. Butler, A.A. Voors, C.S. P. Lam, P. Ponikowski, T. Temple, B. Pieske, J. Ezekowitz, A.F. Hernandez, J. Koglin, C.M. O'Connor, A multicenter, randomized, Double-Blind, Placebo-Controlled trial of the efficacy and safety of the oral soluble guanylate cyclase stimulator, JACC Heart Fail 6 (2018) 96–104, https://doi.org/10.1016/j.jchf.2017.08.013.
[66] J. Rüdebusch, A. Benkner, N. Nath, L. Fleuch, L. Kaderali, K. Grube, K. Klingel, G. Eckstein, T. Meitinger, J. Fielitz, S.B. Felix, Stimulation of soluble guanylyl cyclase (sGC) by riociguat attenuates heart failure and pathological cardiac remodelling, Br. J. Pharm. 179 (2022) 2430–2442, https://doi.org/10.1111/bph.15333.
[67] K. Pradhan, A. Sydykov, X. Tian, A. Mamazhakypov, B. Neupane, H. Luitel, N. Weissmann, W. Seeger, F. Grimminger, A. Kretschmer, J.-P. Stasch, H. A. Ghofrani, R.T. Schermuly, Soluble guanylate cyclase stimulator riociguat and phosphodiesterase 5 inhibitor sildenafil ameliorate pulmonary hypertension due to left heart disease in mice, Int. J. Cardiol. 216 (2016) 85–91, https://doi.org/10.1016/j.ijcard.2016.04.098.
[68] R.L. Benza, E. Grünig, P. Sandner, J.-P. Stasch, G. Simonneau, The nitric oxide–soluble guanylate cyclase–cGMP pathway in pulmonary hypertension: from PDE5 to soluble guanylate cyclase, Eur. Respir. Rev. 33 (2024) 230183, https://doi.org/10.1183/16000617.0183-2023.
[69] M. Follmann, J. Ackerstaff, G. Redlich, F. Wunder, D. Lang, A. Kern, P. Fey, N. Griebenow, W. Kroh, E.-M. Becker-Pelster, A. Kretschmer, V. Geiss, V. Li, A. Straub, J. Mittendorf, R. Jautelat, H. Schirok, K.-H. Schlemmer, K. Lustig, M. Gerisch, A. Knorr, H. Tinel, T. Mondritzki, H. Trübel, P. Sandner, J.-P. Stasch, Discovery of the soluble guanylate cyclase stimulator vericiguat (BAY 1021189) for the treatment of chronic heart failure, J. Me.d Chem. 60 (2017) 5146–5161, https://doi.org/10.1021/acs.jmedchem.7b00449.
[70] T. Harada, H. Kondo, K. Nakamura, Y. He, S. Goto, M. Takahashi, H. Yamasaki, N. Matsuda, M. Takano, I. Abe, A. Fukui, H. Akioka, Y. Teshima, K. Yufu, H. Shibata, N. Takahashi, Soluble guanylate cyclase stimulator vericiguat attenuates angiotensin II-Induced oxidative stress and cardiac remodeling, Circ. J. (2025) CJ-24-0659, https://doi.org/10.1253/circj.CJ-24-0659.
[71] M.A. Caporizzo, B.L. Prosser, The microtubule cytoskeleton in cardiac mechanics and heart failure, Nat. Rev. Cardiol. 19 (2022) 364–378, https://doi.org/10.1038/s41569-022-00692-y.
[72] C.Y. Chen, M.A. Caporizzo, K. Bedi, A. Vite, A.I. Bogush, P. Robison, J.G. Heffler, A.K. Salomon, N.A. Kelly, A. Babu, M.P. Morley, K.B. Margulies, B.L. Prosser, Suppression of detyrosinated microtubules improves cardiomyocyte function in human heart failure, Nat. Med. 24 (2018) 1225–1233, https://doi.org/10.1038/s41591-018-0046-2.
[73] S.A. Phyo, K. Uchida, C.Y. Chen, M.A. Caporizzo, K. Bedi, J. Griffin, K. Margulies, B.L. Prosser, Transcriptional, post-transcriptional, and post-translational mechanisms rewrite the tubulin code during cardiac hypertrophy and failure, Front Cell Dev. Biol. 10 (2022), https://doi.org/10.3389/fcell.2022.837486.
[74] M.E. Wawro, K. Sobierajska, W.M. Ciszewski, W. Wagner, M. Frontczak, K. Wieczorek, J. Niewiarowska, Tubulin beta 3 and 4 are involved in the generation of early fibrotic stages, Cell Signal 38 (2017) 26–38, https://doi.org/10.1016/j.cellsig.2017.06.014.
[75] L. Li, Q. Zhang, X. Zhang, J. Zhang, X. Wang, J. Ren, J. Jia, D. Zhang, X. Jiang, J. Zhang, H. Mei, B. Chen, J. Hu, Y. Huang, Microtubule associated protein 4 phosphorylation leads to pathological cardiac remodeling in mice, EBioMedicine 37 (2018) 221–235, https://doi.org/10.1016/j.ebiom.2018.10.017.
[76] X. Yu, X. Chen, M. Amrute-Nayak, E. Allgeyer, A. Zhao, H. Chenoweth, M. Clement, J. Harrison, C. Doreth, G. Sirinakis, T. Krieg, H. Zhou, H. Huang, K. Tokuraku, D.S. Johnston, Z. Mallat, X. Li, MARK4 controls ischaemic heart failure through microtubule detyrosination, Nature 594 (2021) 560–565, https://doi.org/10.1038/s41586-021-03573-5.
[77] M. Sussman, S. Welch, A. Walker, R. Klevitsky, T. Hewett, S. Witt, T. Kimball, R. Price, H. Lim, J. Molkentin, hypertrophic defect unmasked by calcineurin

expression in asymptomatic tropomodulin overexpressing transgenic mice, Cardiovasc Res. 46 (2000) 90–101, https://doi.org/10.1016/S0008-6363(99)00422-8.
[78] S. Rajan, G. Jagatheesan, C.N. Karam, M.L. Alves, I. Bodi, A. Schwartz, C. F. Bulcao, K.M. D'Souza, S.A. Akhter, G.P. Boivin, D.K. Dube, N. Petrashevskaya, A.B. Herr, R. Hullin, S.B. Liggett, B.M. Wolska, R.J. Solaro, D.F. Wieczorek, Molecular and functional characterization of a novel Cardiac-Specific human tropomyosin isoform, Circulation 121 (2010) 410–418, https://doi.org/10.1161/CIRCULATIONAHA.109.889725.
[79] A.A. Kumar, D.P. Kelly, J.A. Chirinos, Mitochondrial dysfunction in heart failure with preserved ejection fraction, Circulation 139 (2019) 1435–1450, https://doi.org/10.1161/CIRCULATIONAHA.118.036259.
[80] E. Nisoli, E. Clementi, C. Paolucci, V. Cozzi, C. Tonello, C. Sciorati, R. Bracale, A. Valerio, M. Francolini, S. Moncada, M.O. Carruba, Mitochondrial biogenesis in mammals: the role of endogenous nitric oxide, Science 299 (1979) (2003) 896–899, https://doi.org/10.1126/science.1079368.
[81] S. Frankenreiter, P. Bednarczyk, A. Kniess, N.I. Bork, J. Straubinger, P. Koprowski, A. Wrzosek, E. Mohr, A. Logan, M.P. Murphy, M. Gawaz, T. Krieg, A. Szewczyk, V.O. Nikolaev, P. Ruth, R. Lukowski, cGMP-Elevating compounds and ischemic conditioning provide cardioprotection against ischemia and reperfusion injury via Cardiomyocyte-Specific BK channels, Circulation 136 (2017) 2337–2355, https://doi.org/10.1161/CIRCULATIONAHA.117.028723.
[82] D. Fraccarollo, P. Galuppo, S. Motschenbacher, H. Ruetten, A. Schäfer, J. Bauersachs, Soluble guanylyl cyclase activation improves progressive cardiac remodeling and failure after myocardial infarction. Cardioprotection over ACE inhibition, Basic Res Cardiol. 109 (2014) 421, https://doi.org/10.1007/s00395-014-0421-1.
[83] L. Scandalis, D.W. Kitzman, B.J. Nicklas, M. Lyles, P. Brubaker, M.B. Nelson, M. Gordon, J. Stone, J. Bergstrom, P.D. Neufer, E. Gnaiger, A.J.A. Molina, Skeletal muscle mitochondrial respiration and exercise intolerance in patients with heart failure with preserved ejection fraction, JAMA Cardiol. 8 (2023) 575, https://doi.org/10.1001/jamacardio.2023.0957.
[84] M. Meddeb, N. Koleini, A. Binek, M. Keykhaei, R. Darehgazani, S. Kwon, C. Aboaf, K.B. Margulies, K.C. Bedi, M. Lehar, K. Sharma, V.S. Hahn, J.E. Van Eyk, C. I. Drachenberg, D.A. Kass, Myocardial ultrastructure of human heart failure with preserved ejection fraction, Nat. Cardiovasc. Res. 3 (2024) 907–914, https://doi.org/10.1038/s44161-024-00516-x.
[85] F.L. Sheeran, S. Pepe, Posttranslational modifications and dysfunction of mitochondrial enzymes in human heart failure, Am. J. Physiol. Endocrinol. Metab. 311 (2016) E449–E460, https://doi.org/10.1152/ajpendo.00127.2016.
[86] S. Todisco, B. Musio, V. Pesce, M.M. Cavalluzzi, G. Petrosillo, G. La Piana, M. N. Sgobba, N. Schlosserová, L. Cafferati Beltrame, R. Di Lorenzo, V. Tragni, D. Marzulli, L. Guerra, A. De Grassi, V. Gallo, M. Volpicella, L.L. Palese, G. Lentini, C.L. Pierri, Targeting mitochondrial impairment for the treatment of cardiovascular diseases: from hypertension to ischemia-reperfusion injury, searching for new pharmacological targets, Biochem Pharm. 208 (2023) 115405, https://doi.org/10.1016/j.bcp.2022.115405.
[87] T.T. Nielsen, N.B. Stottrup, B. Lofgren, H.E. Botker, Metabolic fingerprint of ischaemic cardioprotection: importance of the malate-aspartate shuttle, Cardiovasc Res 91 (2011) 382–391, https://doi.org/10.1093/cvr/cvr051.
[88] N.M. Niemi, D.J. Pagliarini, The extensive and functionally uncharacterized mitochondrial phosphoproteome, J. Biol. Chem. 297 (2021) 100880, https://doi.org/10.1016/j.jbc.2021.100880.
[89] J. Feng, M. Zhu, M.C. Schaub, P. Gehrig, B. Roschitzki, E. Lucchinetti, M. Zaugg, Phosphoproteome analysis of isoflurane-protected heart mitochondria: phosphorylation of adenine nucleotide translocator-1 on Tyr194 regulates mitochondrial function, Cardiovasc Res 80 (2008) 20–29, https://doi.org/10.1093/cvr/cvn161.
[90] G. Summer, A.R. Kuhn, C. Munts, D. Miranda-Silva, A.F. Leite-Moreira, A. P. Lourenço, S. Heymans, I. Falcão-Pires, M. van Bilsen, A directed network analysis of the cardiome identifies molecular pathways contributing to the development of HFpEF, J. Mol. Cell Cardiol. 144 (2020) 66–75, https://doi.org/10.1016/j.yjmcc.2020.05.008.
[91] M. Wagner, E. Bertero, A. Nickel, M. Kohlhaas, G.E. Gibson, W. Heggermont, S. Heymans, C. Maack, Selective NADH communication from α-ketoglutarate dehydrogenase to mitochondrial transhydrogenase prevents reactive oxygen species formation under reducing conditions in the heart, Basic Res. Cardiol. 115 (2020) 53, https://doi.org/10.1007/s00395-020-0815-1.
[92] B. Qi, L. Song, L. Hu, D. Guo, G. Ren, T. Peng, M. Liu, Y. Fang, C. Li, M. Zhang, Y. Li, Cardiac-specific overexpression of Ndufs1 ameliorates cardiac dysfunction after myocardial infarction by alleviating mitochondrial dysfunction and apoptosis, Exp. Mol. Med 54 (2022) 946–960, https://doi.org/10.1038/s12276-022-00800-5.
[93] V. Adams, A. Schauer, A. Augstein, V. Kirchhoff, R. Draskowski, A. Jannasch, K. Goto, G. Lyall, A. Männel, P. Barthel, N. Mangner, E.B. Winzer, A. Linke, S. Labeit, Targeting MuRF1 by small molecules in a HFpEF rat model improves myocardial diastolic function and skeletal muscle contractility, J. Cachex.. Sarcopenia Muscle 13 (2022) 1565–1581, https://doi.org/10.1002/jcsm.12968.
[94] T. Rubio-Tomás, C. Soler-Botija, O. Martínez-Estrada, J.A. Villena, Transcriptional control of cardiac energy metabolism in health and disease: lessons from animal models, Biochem. Pharm. 224 (2024) 116185, https://doi.org/10.1016/j.bcp.2024.116185.
[95] W.H. Moos, D.V. Faller, I.P. Glavas, D.N. Harpp, N. Kamperi, I. Kanara, K. Kodukula, A.N. Mavrakis, J. Pernokas, M. Pernokas, C.A. Pinkert, W.R. Powers, K. Steliou, C. Tamvakopoulos, D.G. Vavvas, R.J. Zamboni, K. Sampani, Pathogenic mitochondrial dysfunction and metabolic abnormalities, Biochem. Pharm. 193 (2021) 114809, https://doi.org/10.1016/j.bcp.2021.114809.
[96] C. Huang, K. Deng, M. Wu, Mitochondrial cristae in health and disease, Int J. Biol. Macromol. 235 (2023) 123755, https://doi.org/10.1016/j.ijbiomac.2023.123755.
[97] X. Tang, S. Zhao, J. Liu, X. Liu, X. Sha, C. Huang, L. Hu, S. Sun, Y. Gao, H. Chen, Z. Zhang, D. Wang, Y. Gu, S. Chen, L. Wang, A. Gu, F. Chen, J. Pu, X. Chen, B. Yu, L. Xie, Z. Huang, Y. Han, Y. Ji, Mitochondrial GSNOR alleviates cardiac dysfunction via ANT1 denitrosylation, Circ. Res. 133 (2023) 220–236, https://doi.org/10.1161/CIRCRESAHA.123.322654.
[98] N. Narula, M.V. Zaragoza, P.P. Sengupta, P. Li, N. Haider, J. Verjans, K. Waymire, M. Vannan, D.C. Wallace, Adenine nucleotide translocase 1 deficiency results in dilated cardiomyopathy with defects in myocardial mechanics, histopathological alterations, and activation of apoptosis, JACC Cardiovasc Imaging 4 (2011) 1–10, https://doi.org/10.1016/j.jcmg.2010.06.018.
[99] T. Walther, C. Tschöpe, A. Sterner-Kock, D. Westermann, S. Heringer-Walther, A. Riad, A. Nikolic, Y. Wang, L. Ebermann, W.-E. Siems, M. Bader, M. Shakibaei, H.-P. Schultheiss, A. Dörner, Accelerated mitochondrial adenosine Diphosphate/Adenosine triphosphate transport improves Hypertension-Induced heart disease, Circulation 115 (2007) 333–344, https://doi.org/10.1161/CIRCULATIONAHA.106.643296.
[100] L.P. Lee-Glover, T.E. Shutt, Mitochondrial quality control pathways sense mitochondrial protein import, Trends Endocrinol. Metab. 35 (2024) 308–320, https://doi.org/10.1016/j.tem.2023.11.004.
[101] Y. Feng, Y. Lu, The nuclear-mitochondrial crosstalk in aging: from mechanisms to therapeutics, Free Radic. Biol. Med. 232 (2025) 391–397, https://doi.org/10.1016/j.freeradbiomed.2025.03.012.
[102] A. Marada, C. Walter, T. Suhm, S. Shankar, A. Nandy, T. Brummer, I. Dhaouadi, F.-N. Vögtle, C. Meisinger, DYRK1A signalling synchronizes the mitochondrial import pathways for metabolic rewiring, Nat. Commun. 15 (2024) 5265, https://doi.org/10.1038/s41467-024-49611-4.
[103] P. Latorre-Muro, T. Vitale, M. Ravichandran, K. Zhang, J.M. Palozzi, C.F. Bennett, A. Lamas-Paz, J.H. Sohn, T.D. Jackson, M. Jedrychowski, S.P. Gygi, S. Kajimura, A. Schmoker, H. Jeon, M.J. Eck, P. Puigserver, Chaperone-mediated insertion of mitochondrial import receptor TOM70 protects against diet-induced obesity, Nat. Cell Biol. 27 (2025) 130–140, https://doi.org/10.1038/s41556-024-01555-z.
[104] N. Liu, B. Pang, L. Kang, D. Li, X. Jiang, C. Zhou, TUFM in health and disease: exploring its multifaceted roles, Front. Immunol. 15 (2024), https://doi.org/10.3389/fimmu.2024.1424385.
[105] E.C. Koc, C.A. Hunter, H. Koc, Phosphorylation of mammalian mitochondrial EF-Tu by fyn and c-Src kinases, Cell Signal 101 (2023) 110524, https://doi.org/10.1016/j.cellsig.2022.110524.
[106] H. He, M. Chen, N.K. Scheffler, B.W. Gibson, L.L. Spremulli, R.A. Gottlieb, Phosphorylation of mitochondrial elongation factor tu in ischemic myocardium, Circ. Res 89 (2001) 461–467, https://doi.org/10.1161/hh1701.096038.
[107] J.F. Garbincius, J.W. Elrod, Mitochondrial calcium exchange in physiology and disease, Physiol. Rev. 102 (2022) 893–992, https://doi.org/10.1152/physrev.00041.2020.
[108] B. Roman, Y. Mastoor, J. Sun, H. Chapoy Villanueva, G. Hinojosa, D. Springer, J. C. Liu, E. Murphy, MICU3 regulates mitochondrial calcium and cardiac hypertrophy, Circ. Res. 135 (2024) 26–40, https://doi.org/10.1161/CIRCRESAHA.123.324026.
[109] M. Paillard, K.-T. Huang, D. Weaver, J.P. Lambert, J.W. Elrod, G. Hajnóczky, Altered composition of the mitochondrial Ca2+uniporter in the failing human heart, Cell Calcium 105 (2022) 102618, https://doi.org/10.1016/j.ceca.2022.102618.
[110] A. Yoshii, T.S. McMillen, Y. Wang, B. Zhou, H. Chen, D. Banerjee, M. Herrero, P. Wang, N. Muraoka, W. Wang, C.E. Murry, R. Tian, Blunted cardiac mitophagy in response to metabolic stress contributes to HFpEF, Circ. Res. 135 (2024) 1004–1017, https://doi.org/10.1161/CIRCRESAHA.123.324103.
[111] H. Tsutsui, S. Kinugawa, S. Matsushima, Mitochondrial oxidative stress and dysfunction in myocardial remodelling, Cardiovasc Res. 81 (2008) 449–456, https://doi.org/10.1093/cvr/cvn280.
[112] I. Andreadou, P. Efentakis, K. Frenis, A. Daiber, R. Schulz, Thiol-based redox-active proteins as cardioprotective therapeutic agents in cardiovascular diseases, Basic Res Cardiol. 116 (2021) 44, https://doi.org/10.1007/s00395-021-00885-5.
[113] S.K. Sonn, E.J. Song, S. Seo, Y.Y. Kim, J.-H. Um, F.J. Yeo, D.S. Lee, S. Jeon, M.-N. Lee, J. Jin, H.Y. Kweon, T.K. Kim, S. Kim, S.H. Moon, S.G. Rhee, J. Chung, J. Yang, J. Han, E.-Y. Choi, S.B. Lee, J. Yun, G.T. Oh, Peroxiredoxin 3 deficiency induces cardiac hypertrophy and dysfunction by impaired mitochondrial quality control, Redox Biol. 51 (2022) 102275, https://doi.org/10.1016/j.redox.2022.102275.
[114] S. Reina, S.C. Nibali, M.F. Tomasello, A. Magrì, A. Messina, V. De Pinto, Voltage dependent anion channel 3 (VDAC3) protects mitochondria from oxidative stress, Redox Biol. 51 (2022) 102264, https://doi.org/10.1016/j.redox.2022.102264.
[115] G. Ito, Y. Tatara, K. Itoh, M. Yamada, T. Yamashita, K. Sakamoto, T. Nozaki, K. Ishida, Y. Wake, T. Kaneko, T. Fukuda, E. Sugano, H. Tomita, T. Ozaki, Novel dicarbonyl metabolic pathway via mitochondrial ES1 possessing glyoxalase III activity, BBA Adv. 3 (2023) 100092, https://doi.org/10.1016/j.bbadva.2023.100092.
[116] J. Seth, S. Sharma, C.J. Leong, S.W. Rabkin, Eicosapentaenoic acid (EPA) and docosahexaenoic acid (DHA) ameliorate heart failure through reductions in oxidative stress: a systematic review and Meta-Analysis, Antioxidants 13 (2024) 955, https://doi.org/10.3390/antiox13080955.
[117] R. Liu, W. Li, B. Tao, X. Wang, Z. Yang, Y. Zhang, C. Wang, R. Liu, H. Gao, J. Liang, W. Yang, Tyrosine phosphorylation activates 6-phosphogluconate

dehydrogenase and promotes tumor growth and radiation resistance, Nat. Commun. 10 (2019) 991, https://doi.org/10.1038/s41467-019-08921-8.
[118] T. TeSlaa, M. Ralser, J. Fan, J.D. Rabinowitz, The pentose phosphate pathway in health and disease, Nat. Metab. 5 (2023) 1275–1289, https://doi.org/10.1038/s42255-023-00863-2.
[119] A. Zoccarato, I. Smyrnias, C.M. Reumiller, A.D. Hafstad, M. Chong, D.A. Richards, C.X.C. Santos, A. Visnagri, S. Verma, D.I. Bromage, M. Zhang, X. Zhang, G. Sawyer, R. Thompson, A.M. Shah, NRF2 activation in the heart induces glucose metabolic reprogramming and reduces cardiac dysfunction via upregulation of the pentose phosphate pathway, Cardiovasc Res (2024), https://doi.org/10.1093/cvr/cvae250.
[120] H. He, R.M. Mulhern, W.M. Oldham, W. Xiao, Y.-D. Lin, R. Liao, J. Loscalzo, L-2-Hydroxyglutarate protects against cardiac injury via metabolic remodeling, Circ. Res. 131 (2022) 562–579, https://doi.org/10.1161/CIRCRESAHA.122.321227.
[121] S. Chen, Y. Zou, C. Song, K. Cao, K. Cai, Y. Wu, Z. Zhang, D. Geng, W. Sun, N. Ouyang, N. Zhang, Z. Li, G. Sun, Y. Zhang, Y. Sun, Y. Zhang, The role of glycolytic metabolic pathways in cardiovascular disease and potential therapeutic approaches, Basic Res. Cardiol. 118 (2023) 48, https://doi.org/10.1007/s00395-023-01018-w.
[122] N. Koleini, M. Meddeb, L. Zhao, M. Keykhaei, S. Kwon, F. Farshidfar, V.S. Hahn, E.L. Pearce, K. Sharma, D.A. Kass, Landscape of glycolytic metabolites and their regulating proteins in myocardium from human heart failure with preserved ejection fraction, Eur. J. Heart Fail (2024), https://doi.org/10.1002/ejhf.3389.
[123] X. Wang, G. Zhang, S. Dasgupta, E.L. Niewold, C. Li, Q. Li, X. Luo, L. Tan, A. Ferdous, P.L. Lorenzi, B.A. Rothermel, T.G. Gillette, C.M. Adams, P.E. Scherer, J.A. Hill, Z.V. Wang, ATF4 protects the heart from failure by antagonizing oxidative stress, Circ. Res. 131 (2022) 91–105, https://doi.org/10.1161/CIRCRESAHA.122.321050.
[124] L.Y.M. Michel, H. Esfahani, D. De Mulder, R. Verdoy, J. Ambroise, V. Roelants, B. Bouchard, N. Fabian, J. Savary, J.P. Dewulf, T. Doumont, C. Bouzin, V. Haufroid, J.J.F.P. Luiken, M. Nabben, M.L. Singleton, L. Bertrand, M. Ruiz, C. Des Rosiers, J.-L. Balligand, An NRF2/β3-Adrenoreceptor axis drives a sustained antioxidant and metabolic rewiring through the Pentose-Phosphate pathway to alleviate cardiac stress, Circulation 151 (2025) 1312–1328, https://doi.org/10.1161/CIRCULATIONAHA.124.067876.
[125] T. Wang, M. Ning, Y. Mo, X. Tian, Y. Fu, I. Laher, S. Li, Metabolomic profiling reveals that exercise lowers biomarkers of cardiac dysfunction in rats with type 2 diabetes, Antioxidants 13 (2024) 1167, https://doi.org/10.3390/antiox13101167.